RSC Advances

PAPER

View Article Online
View Journal | View Issue

Check for updates

Cite this: *RSC Adv.*, 2024, **14**, 10464

# Novel pyrazole and imidazolone compounds: synthesis, X-ray crystal structure with theoretical investigation of new pyrazole and imidazolone compounds anticipated insecticide's activities against *targeting Plodia interpunctella* and *nilaparvata lugens*†

Mona A. Shalaby,[b] Mohammad H. BinSabt,[b] Sameh A. Rizk[a] and Asmaa M. Fahim *[c]

In this study, we synthesized (2-propoxyphenyl)(3-(*p*-tolyl)oxiran-2-yl)methanone through oxidizing the double bond of the respective chalcone *via* the Weitz–Scheffer epoxidation reaction. Additionally, the chalcone with an oxirane ring served as a fundamental building block for the synthesis of various pyrazole and imidazole derivatives, employing diverse nitrogen nucleophiles. All synthesized compounds were confirmed *via* analytical and spectroscopic analysis, such as FT-IR, $^{1}$H NMR, $^{13}$C NMR, and mass spectroscopy. Furthermore, all these nitrogen heterocycles were optimized *via* the DFT/B3LYP/6-31G(d,p) basis set and their physical descriptors were identified. Compound **11** was further confirmed using single-crystal X-ray diffraction with Hirshfeld analysis, and the results were correlated with the optimized structure by comparing their bond length and bond angle, which provided excellent correlation. Additionally, the insecticidal activities of the newly synthesized compounds were tested against *P. interpunctella* and *Nilaparvata lugens*. The heterocyclic compounds exhibited remarkable activity compared to the standard reference thiamethoxam. These findings were further confirmed through docking simulation with different proteins, namely PDBID 3aqy and 3wyw. The compounds interacted effectively within the protein pockets, displaying a higher binding energy with amino acids.

Received 23rd January 2024
Accepted 11th March 2024

DOI: 10.1039/d4ra00602j

rsc.li/rsc-advances

Open Access Article. Published on 02 April 2024. Downloaded on 2/13/2026 1:16:18 AM.
This article is licensed under a Creative Commons Attribution-NonCommercial 3.0 Unported Licence.

## 1. Introduction

The multifaceted activities of oxiranes and their derivatives in terms of anti-microbial, anti-cancer, and anti-tumor have been investigated by bio-chemists and chemists.[1–5] For synthesis of oxiranes from chalcones and alkenes, numerous reagents and catalysts have been utilized.[6] These epoxides are flexible chemicals that can easily undergo stereospecific ring-opening reactions to generate multifunctional molecules.[7] Alkene epoxidation is one of the most widespread asymmetric transformations where epoxides serve as intermediates for bioactive target molecules that reflect the efficacy of current epoxidation protocols.[8] Additionally, they serve as monomers for the construction of polymer materials, including epoxy resin and polyether.[9] Through the epoxidation of α,β-unsaturated ketones, the ethylenic bridge was replaced with an oxirane ring.

Considering the infestations of pests causing significant financial losses in storage and agricultural environments, crop horticulture and agricultural protection require insecticides that are important, effective, and widely utilized to achieve high quality and improved yields of produce by fighting insect pests.[10] Many insect pests attack rice crops throughout the growing season—from seed germination till harvesting. Fighting insects is crucial to reduce food loss from stored items due to insect attacks. *P. interpunctella* was one of seven insect species whose eggs were found in brown rice. Prenol, isoprenol, dimethyl disulfide, and dimethyl trisulfide were among the volatile substances produced as a result of the *P. interpunctella* infestation of brown rice. These volatiles have the potential to serve as early biomarkers of insect detection in brown rice.[11] *Planthoppers* or *Nilaparvata lugens* are the most destructive insect pests because they consume rice plant sap, thus causing plant dehydration and transmitting viral diseases.[12] There is a worldwide distribution of these insects. With long-term exposure, insects have developed resistance to a majority of chemical classes used in animal

[a]*Chemistry Department, Faculty of Science, Ain Shams University, Abbassia, P.O. 11566, Cairo, Egypt*

[b]*Chemistry Department, Faculty of Science, University of Kuwait, P.O. Box 5969, Safat, 13060, Kuwait*

[c]*Green Chemistry Department, National Research Centre Dokki, P.O. Box 12622, Cairo, Egypt. E-mail: asmaamahmoud8521@gmail.com*

† Electronic supplementary information (ESI) available. CCDC 2310940. For ESI and crystallographic data in CIF or other electronic format see DOI: https://doi.org/10.1039/d4ra00602j



© 2024 The Author(s). Published by the Royal Society of Chemistry

Open Access Article. Published on 02 April 2024. Downloaded on 2/13/2026 1:16:18 AM.
This article is licensed under a Creative Commons Attribution-NonCommercial 3.0 Unported Licence.

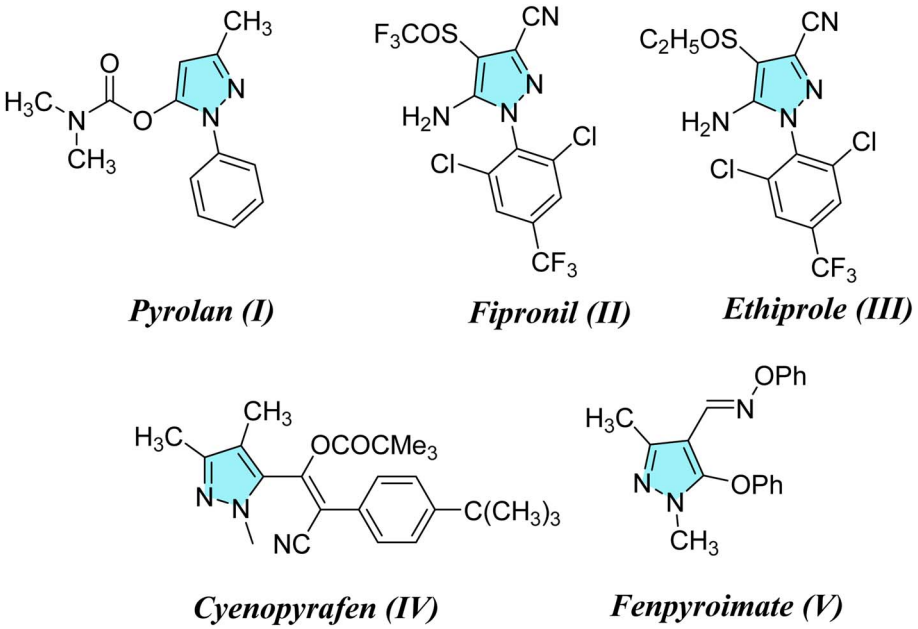


Fig. 1 Agrochemicals containing pyrazole scaffolds.

agriculture and public health. Insecticides are essential for the management of insects and pests and are regarded as one of the most significant barriers to applying unique chemical and biological features as well as good safety profiles with relatively low risk for non-target organisms in the environment. Their investigated exposure strategies were flexible and had a low application rate as well as excellent absorption and translocation in plants. Thus, there is a need to find insecticides that combat these insects.[13–15] Many pyrazole compounds have been reported to be effective insecticides. Pyrolan (**I**), fipronil (**II**), ethiprole (**III**), cyenopyrafen (**IV**) and fenpyroximate (**V**) (Fig. 1) are examples of pyrazole insecticides with high insecticidal activity on the market today.[16–19] On the other hand, in agrochemicals, imidazole is widely incorporated as a nitrogen-containing aromatic heterocycle, as shown in Fig. 2.[20–22] Prochloraz (**VI**), for example, is an imidazole fungicide that is widely used in gardening and agriculture. It is applied to wheat, barley, mushrooms, cherries, golf course turf, and flower production. Imidacloprid (IMI) (**VII**) is a neonicotinoid insecticide that is used for crop protection all over the world. In this study, various pyrazole and imidazole derivatives were successfully synthesized and fully characterized using analytical and spectroscopic techniques. Furthermore, theoretical studies were carried out for nitrogen heterocycles to determine their physical properties. Moreover, this study examines the insecticidal activities of newly synthesized pyrazole and imidazole derivatives against *P. interpunctella* and *Nilaparvata lugens*. The results were further supported by docking simulations involving various proteins.

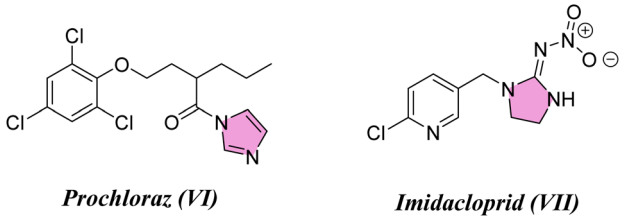


Fig. 2 Agrochemicals containing imidazole scaffolds.

## 2. Results and discussion

### 2.1. Chemistry section

The reaction of 2-(5-(*p*-tolyl)-4,5-dihydro-1*H*-pyrazol-3-yl)phenol (**1**) with sodium hydroxide/hydrogen peroxide-mediated in acetone and methanol as a solvent did not form the corresponding epoxy compound **2** and formed the C-4′-substituted flavonol **3**, as shown in Scheme 1.[23]

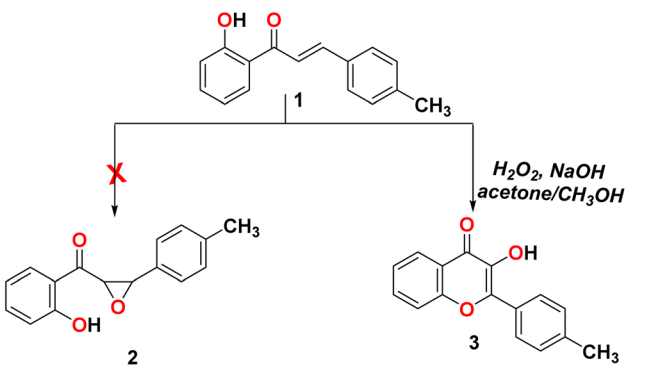


Scheme 1 Reactivity of 2-(5-(*p*-tolyl)-4,5-dihydro-1*H*-pyrazol-3-yl) phenol (**1**) with $H_2O_2$.

Open Access Article. Published on 02 April 2024. Downloaded on 2/13/2026 1:16:18 AM.
This article is licensed under a Creative Commons Attribution-NonCommercial 3.0 Unported Licence.

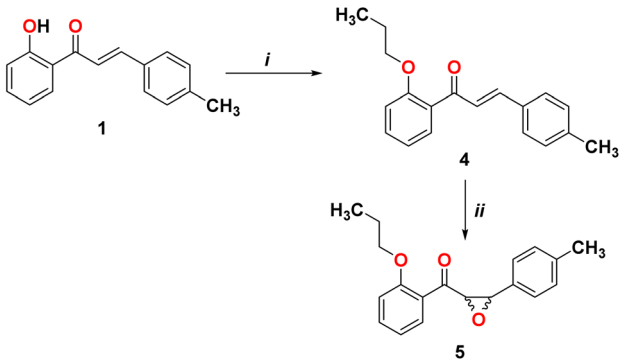


Scheme 2 Reagents and conditions. (i) $Br(CH_2)_2CH_3$, $K_2CO_3$, and DMF; (ii) $H_2O_2$, NaOH, acetone, and $CH_3OH$.

In order to form the epoxide compound, we blocked the OH group in the chalcone compound **1** using alkyl halide, as shown in Scheme 2.

We start converting chalcone **1** to chalcone **4** by the reaction with bromopropane in order to block the OH group. A racemic form of epoxychalcone **5** has been obtained by oxidizing the double bonds of the respective chalcone **4** in a solution of 30% hydrogen peroxide in an alkaline medium *via* the Weitz–Scheffer epoxidation reaction.[24,25] Elemental analysis, IR, NMR, and mass spectroscopy were used to confirm the oxirane product **5**. Two doublet signals were detected in the $^1$HNMR spectrum of compound **5** at 4.00 ppm and at 4.49 ppm, which correspond to the oxirane ring.

Pyrazines can be obtained through the cyclo-condensation of hydrazines with dicarbonyl compounds (Knorr's method)[26] and by cycloaddition between alkenes or alkynes and dipolar compounds.[27,28] As a nucleophilic reagent, hydrazine hydrate and phenyl hydrazine derivatives were used to perform nucleophilic reaction on epoxychalcone **5**. Reacting α,β-epoxyketone **5** with hydrazine hydrate **6** or phenyl hydrazine **8a** in boiling ethanol led to the formation of 4,5-dihydro-1*H*-pyrazol-4-ol derivatives **7** and **9**, respectively. However, when epoxychalcones **5** are reacted with phenylhydrazine hydrochloride **8b** and **8c** under the same conditions, they give the corresponding *N*-phenyl pyrazolo derivatives **10** and **11** (Scheme 3). In order to monitor the reaction progress, TLC was used. FT-IR and $^1$H/$^{13}$C NMR spectra analyses confirmed their chemical structures. The FT-IR spectrum of phenylpyrazol-4-ol **7**, **9**, and **10** showed broadened stretch bands at 3157, 3538, and 3317 $cm^{-1}$ for the OH group, respectively, in addition to the stretching band at 3263 $cm^{-1}$ due to the NH group in compound **7**. Also, the IR spectra for these compounds showed bands at about 1595 $cm^{-1}$ due to the C=N group. Based on the $^1$HNMR spectra of compounds **7–10**, the signals corresponding to the hydroxyl group, C4 proton, and C5 proton were detected in the pyrazole ring. In addition, compound **11** was confirmed using single-crystal X-ray diffraction.

Many natural products and pharmaceutically active compounds contain imidazolone scaffolds. Also, several substituted imidazolones have received considerable attention due to their diverse medicinal applications. On the other hand, hydantoin derivatives are used in polymer chemistry, medicine, and the chemical industry.[29–32] In order to generate new substances that have potential pharmacological or medicinal applications, epoxy-chalcone was used as a part of our research program directed toward designing and synthesizing compounds for potentially interesting bioactive compounds. Interestingly, when we treated epoxy chalcone **5** with guanidine hydrochloride in the presence of potassium hydroxide in

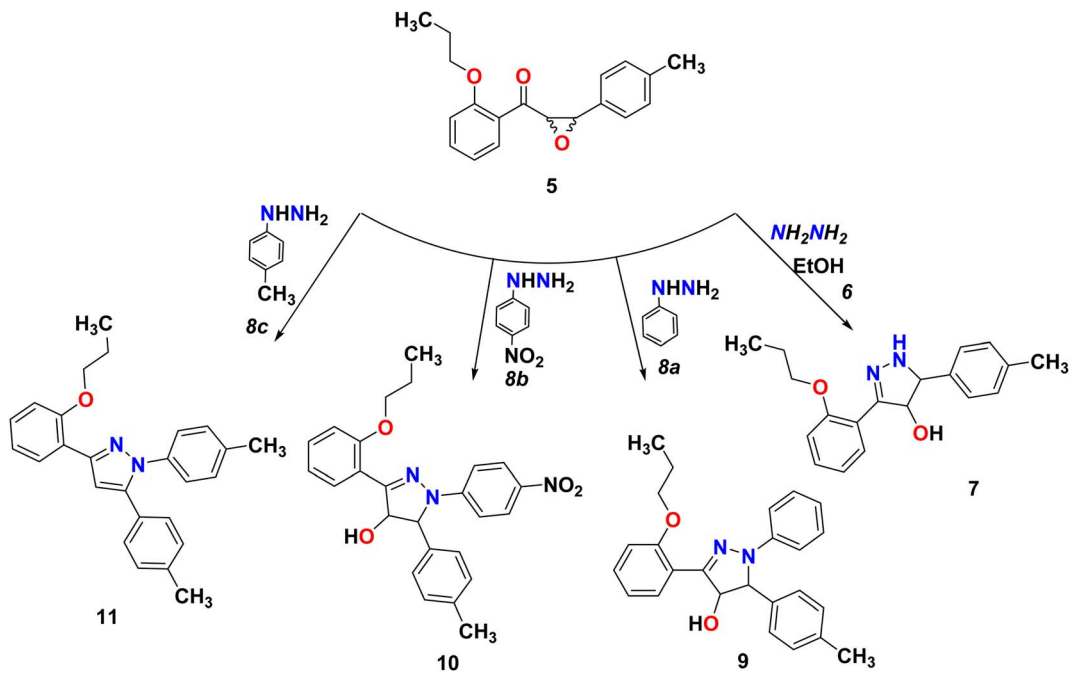


Scheme 3 Reaction of epoxychalcone **5** with hydrazine hydrate **6** and phenyl hydrazine **8a–c** refluxed for 3 hours in ethanol as a solvent.


© 2024 The Author(s). Published by the Royal Society of Chemistry

Open Access Article. Published on 02 April 2024. Downloaded on 2/13/2026 1:16:18 AM.
This article is licensed under a Creative Commons Attribution-NonCommercial 3.0 Unported Licence.

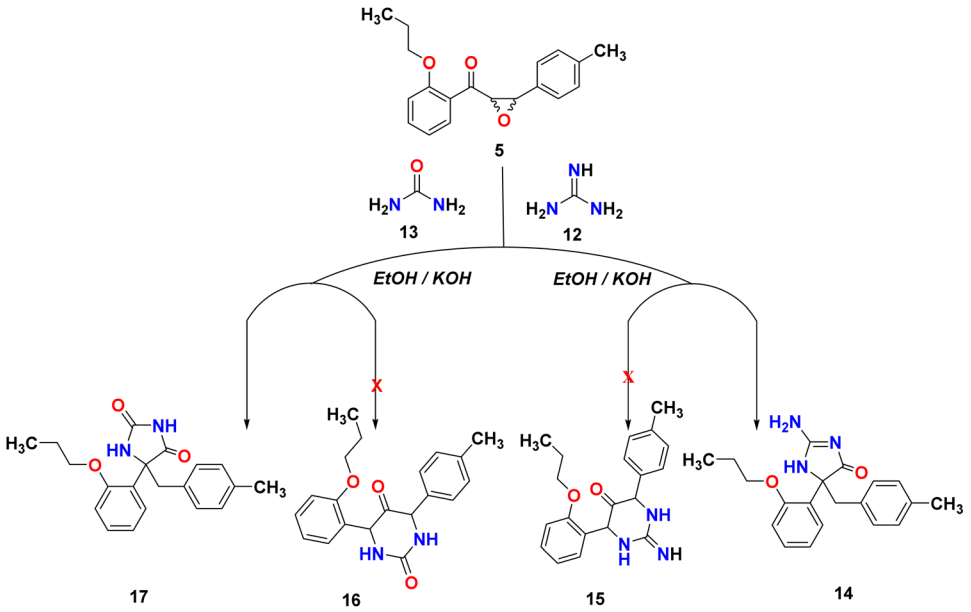


Scheme 4 Reactivity of epoxy-chalcone **5** with guanidine hydrochloride and urea.

ethanol (Scheme 4), the imidazolone compound **14** was formed instead of the pyrimidinone **15**. Also, the reaction of epoxychalcone **5** with urea in the presence of potassium hydroxide in ethanol (Scheme 4) afforded the imidazolone compound **17** instead of the pyrimidinone **16**. The IR spectrum of compound **14** showed characteristic stretching bands at 3265, 3055, 1656,

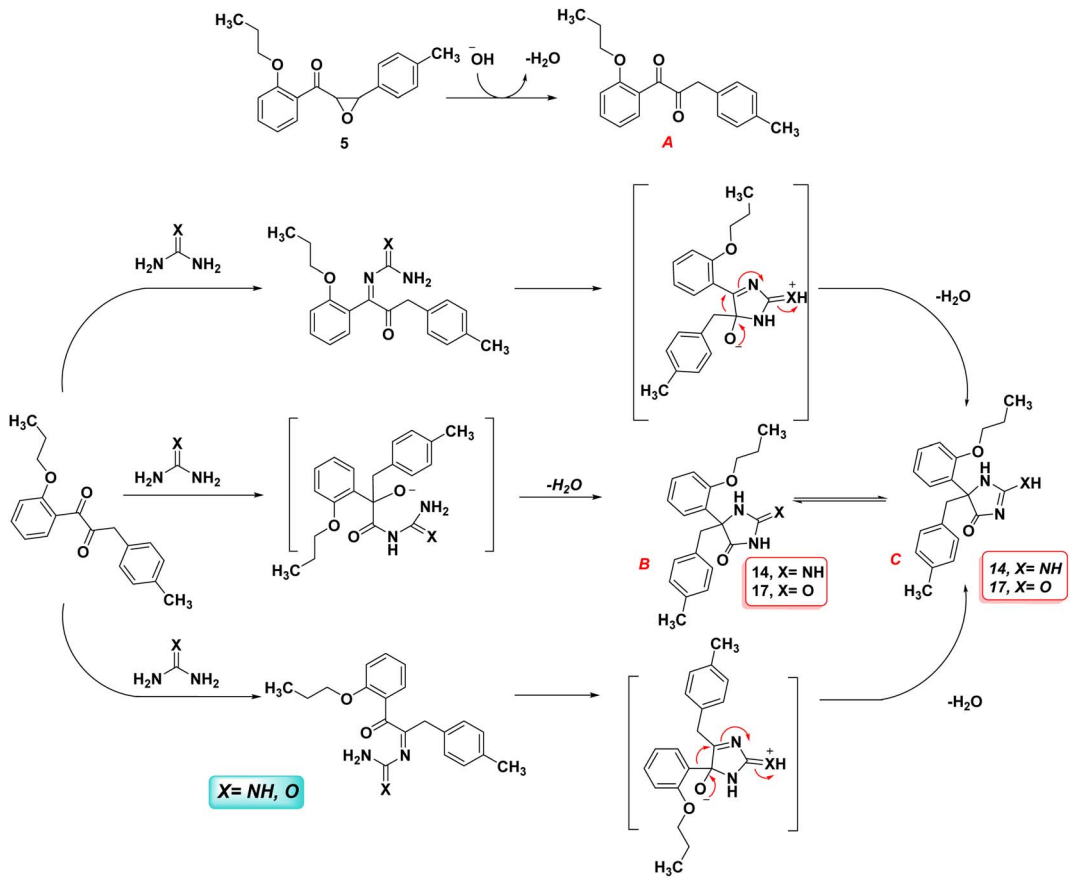


Scheme 5 Plausible mechanism of the formation of imidazolone compound **14** and **17**.

Open Access Article. Published on 02 April 2024. Downloaded on 2/13/2026 1:16:18 AM.
This article is licensed under a Creative Commons Attribution-NonCommercial 3.0 Unported Licence.

and 1598 $cm^{-1}$ due to NH, aromatic C–H, C=O, and C=N groups, respectively, whereas for compound **17**, the IR spectrum showed bands at 3356, 3068, and 1763 $cm^{-1}$ due to aromatic NH, aromatic C–H, and C=O groups, respectively. The two compounds **14** and **17** showed two doublets in $^1$H-NMR at $\delta$ 2.92, 3.18 ppm for $H_A$ and 3.32, 3.40 for $H_B$ of the $CH_2$ group, respectively. Additionally, compound **14** showed a $D_2O$ exchangeable singlet peak of NH at 7.37 ppm, while compound **17** showed an exchangeable singlet two peaks at 7.85 and 10.09 ppm, respectively. The chemical shifts of all other aromatic protons were observed in accordance with expectations. Molecular ions from compounds **14** and **17** exhibited peaks at *m*/*z* 337 and 338, respectively, in the mass spectrum, as shown in Scheme 4.

Scheme 5 illustrates a possible mechanism for the formation of hydantoin. As in various base-catalyzed reactions of 2,3-epoxydiphenyl ketones,[32,33] the first step is the isomerization of the chalcone-epoxide **5** to the corresponding 1,2-dione (**A**). There are two major pathways that can be envisaged from the intermediate 1,2-dione (**A**). First, a similar reaction to a benzil-benzilic acid rearrangement occurs when the *N*-atom of guanidine or urea attacks one of the carbonyl carbons, thereby initiating the migration of an aryl (or aryl–methyl) towards the rearranged products **B** or **C**. However, the more stable and final product in the case of urea is hydantoin compound **B**, while hydantoin compound **C** is in the case of guanidine. Second, the 1,2-dione may also form 5-membered ring-closed intermediates as the result of condensation products that lead to identical rearranged products **B** and **C** *via* the aryl (or aryl–methyl) migration. Regardless of which groups migrate, both feasible pathways end up producing the same product; therefore, the two isomeric intermediates are possible.

## 2.2. DFT investigation

**2.2.1. Physical descriptor's.** All produced compounds **7**, **9**, **10**, **11**, **14** and **17** as well as epoxychalcone **5** were fully optimized using the DFT/B3LYP/6-31G(d,p) basis set,[34–36] as shown in Fig. 3. Frequency calculations are performed to ensure that there are no imaginary frequencies. Table 1 shows the physical properties used to optimize the molecular structures of all compounds, which include ($\sigma$) absolute softness, ($\chi$) electronegativity, ($\Delta N_{max}$) electronic charge, ($\eta$) absolute hardness, ($\omega$) global electrophilicity, ($S$) global softness, and (Pi) chemical potential based on eqn (1)–(8) calculated by B3LYP/6-31G(d,p).

$$\Delta E = E_{LUMO} - E_{HOMO} \quad (1)$$

$$\chi = \frac{-(E_{HOMO} + E_{LUMO})}{2} \quad (2)$$

$$\mu = \frac{(E_{LUMO} - E_{HOMO})}{2} \quad (3)$$

$$\sigma = 1/\eta \quad (4)$$

$$Pi = -\chi \quad (5)$$

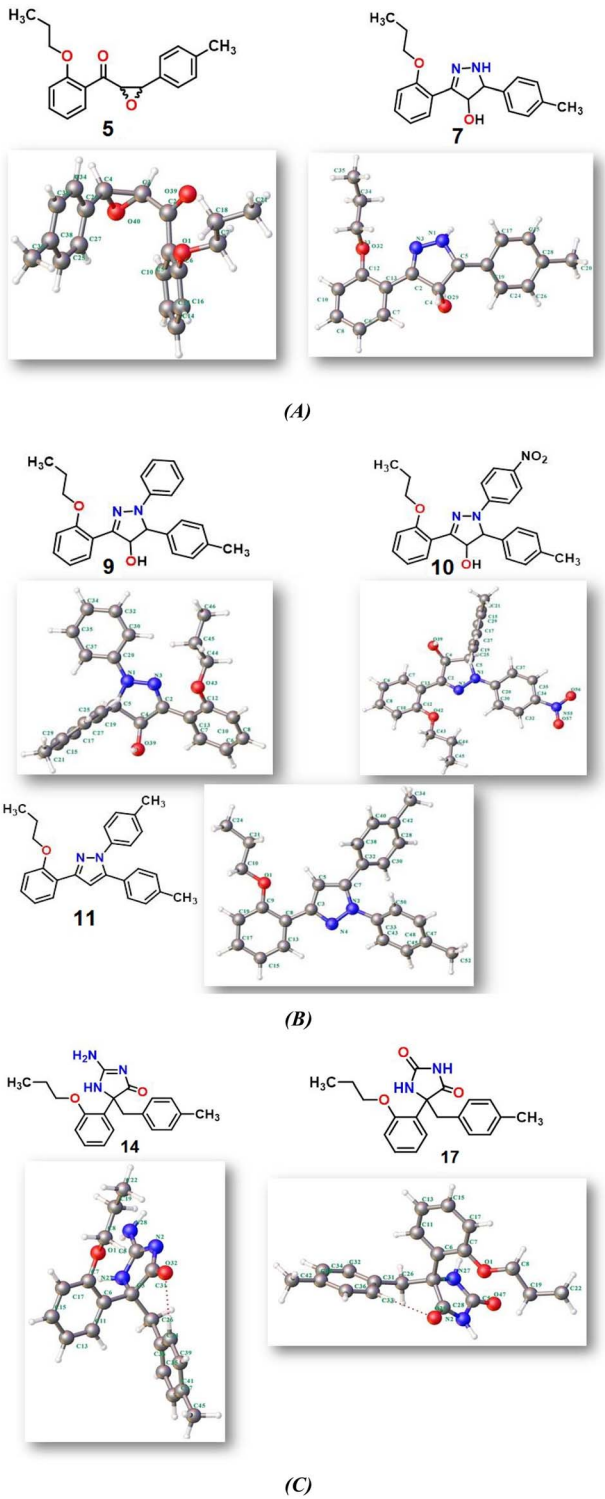


Fig. 3 (A–C) Chemical and the optimized structure of compounds **5**, **7**, **9**, **10**, **11**, **14** and **17** utilizing the DFT/6-31(G) basis set.

$$S = 1/2\eta \quad (6)$$

$$\omega = Pi^2/2\eta \quad (7)$$

$$\Delta N_{max} = -Pi/\eta \quad (8)$$


© 2024 The Author(s). Published by the Royal Society of Chemistry

Open Access Article. Published on 02 April 2024. Downloaded on 2/13/2026 1:16:18 AM. This article is licensed under a Creative Commons Attribution-NonCommercial 3.0 Unported Licence.

Table 1 Ground state energies of compound **5**, **7**, **9**, **10**, **11**, **14** and **17** utilizing DFT/B3LYP/6-31G(d,p) and their physical parameters

| Physical descriptors | | | | | | | | | | | | |
|---|---|---|---|---|---|---|---|---|---|---|---|---|
| Compound | $E_T$ (au) | $E_{HOMO}$ (eV) | $E_{LUMO}$ (e V) | $E_g$ (eV) | $\mu$ (D) | $\chi$ (eV) | $\eta$ (eV) | $\sigma$ (eV) | Pi (eV) | $S$ (eV) | $\omega$ (eV) | $\Delta N_{max}$ |
| **5** | −961.71 | −6.282 | −1.479 | 4.803 | 1.46 | 3.881 | 2.401 | 0.416 | −3.881 | 0.208 | 3.136 | 1.616 |
| **7** | −997.20 | −5.499 | −0.969 | 4.530 | 1.69 | 3.234 | 2.265 | 0.441 | −3.234 | 0.220 | 2.308 | 1.427 |
| **9** | −1228.27 | −4.907 | −1.103 | 3.804 | 1.33 | 1.333 | 1.901 | 0.525 | −3.005 | 0.262 | 2.374 | 1.580 |
| **10** | −1432.78 | −5.336 | −1.895 | 3.441 | 7.92 | 3.616 | 1.720 | 0.581 | −3.616 | 0.290 | 3.800 | 2.101 |
| **11** | −1191.19 | −5.276 | −0.724 | 4.552 | 2.77 | 3.000 | 2.275 | 0.439 | −3.000 | 0.219 | 1.977 | 1.318 |
| **14** | −1090.73 | −5.938 | −0.267 | 5.671 | 5.14 | 3.103 | 2.835 | 0.352 | −3.103 | 0.176 | 1.698 | 1.094 |
| **17** | −1110.62 | −6.155 | −0.412 | 5.743 | 2.76 | 3.284 | 2.871 | 0.348 | −3.284 | 0.174 | 1.877 | 1.143 |

Fig. 3 shows the results of full optimization using the DFT/B3LYP/6-31G(d,p) basis set for all generated compounds **7–17** including epoxy **5**. Table 2 lists the physical properties used in the optimization of molecular structures of all compounds with regard to ($\sigma$) absolute softness, ($\chi$) electronegativity, ($\Delta N_{max}$) electronic charge, ($\eta$) absolute hardness, ($\omega$) global electrophilicity, ($S$) global softness, and (Pi) chemical potential based on eqn (1)–(8) estimated from B3LYP/6-31G(d,p). The total energies of compounds **7–17** were more stable overall than the initial epoxy chalcone **5**, indicating their stability. Compound **10** also demonstrated greater stability, with an energy of (−1432.78 au) (−38987.84 eV), which can be attributed to the presence of 4O and 3N in its structure, which increases the compound's electronegativity. Additionally, compared to other compounds, compound **10** has an extremely large dipole moment. Compound **10** and epoxy chalcone **5** have dipole moments that differ by 6.46 D. This is due to the presence of a nitro group, which makes it easier to separate charges and increase reactivity. Table 1 indicates that compound **17** has a higher hardness of 2.87 eV and a low softness of 0.34 eV, suggesting a lower intramolecular charge transfer. Also, compound **17** exhibits the greatest $\Delta E$, indicating its superior kinetic stability when compared to other compounds. On the other hand, compound **10** displays the lowest $\Delta E$, signifying its heightened chemical reactivity. HOMO–LUMO orbitals are illustrated in Fig. 4, and their orbital analyses at the B3LYP/6-31G(d,p) level for compounds **5–17** are shown in Fig. 5. A positive phase was characterized by red colors, while a negative phase was characterized by green colors. Compound **5** has a HOMO with electron clouds mostly over the tolyl ring, epoxy group, and oxygen atom of the ketone group, whereas its LUMO is charged throughout the molecule except for the tolyl group and alkyl group. For the synthesized heterocyclic compounds, the electron clouds in HOMO and LUMO of compound **7** distribute charges over the entire molecule except for the tolyl and alkyl groups. Additionally, the HOMO and LUMO of compound **9** and compound **10** showed a similar charge distribution with the

Table 2 Crystal data and refinement parameters of compound **11** (CCDC: 2310940)

| Crystal data of compound **11** | |
|---|---|
| Chemical formula | $C_{26}H_{26}N_2O$ |
| $M_r$ | 382.49 |
| Crystal system, space group | Monoclinic, $P2_1/n$ |
| Temperature (K) | 296 |
| $a$, $b$, $c$ (Å) | 6.7814 (4), 10.6880 (7), 29.8384 (18) |
| $\beta$ (°) | 94.276 (3) |
| $V$ (Å$^3$) | 2156.7 (2) |
| $Z$ | 4 |
| Radiation type | Cu K$\alpha$ |
| $\mu$ (mm$^{-1}$) | 0.56 |
| Crystal size (mm) | 0.21 × 0.16 × 0.11 |
| Diffractometer | Bruker APEX-II CCD |
| Absorption correction | Multi-scan SADABS2016/2 – Bruker AXS area detector scaling and absorption correction |
| $T_{min}$, $T_{max}$ | 0.89, 0.94 |
| No. of measured, independent & observed [$I > 2\sigma(I)$] reflections | 14 524, 3725, 3159 |
| $R_{int}$ | 0.029 |
| $(\sin\theta/\lambda)_{max}$ (Å$^{-1}$) | 0.595 |
| $R[F^2 > 2\sigma(F^2)]$, $wR(F^2)$, $S$ | 0.040, 0.125, 1.06 |
| No. of reflections | 3725 |
| No. of parameters | 265 |
| H-atom treatment | Constrained |
| $\Delta\rho_{max}$, $\Delta\rho_{min}$ (e Å$^{-3}$) | 0.14, −0.12 |

Open Access Article. Published on 02 April 2024. Downloaded on 2/13/2026 1:16:18 AM.
This article is licensed under a Creative Commons Attribution-NonCommercial 3.0 Unported Licence.

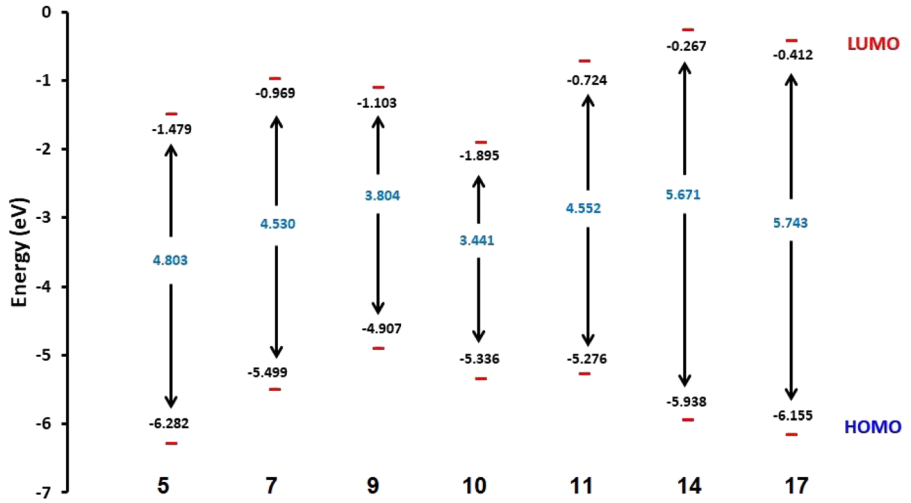


Fig. 4 Schematic diagrams of HOMO and LUMO energy levels of compounds **5**, **7**, **9**, **10**, **11**, **14** and **17** obtained from the DFT calculation with the B3LYP/6-31G(d,p) basis set.

exception of the tolyl group and alkyl group. The HOMO of compound **11** displays electron clouds that are distributed across the entirety of the molecule with the exception of the two methyl and alkyl groups, while the LUMO distributes charges throughout the molecule except for the two methyl and alkoxy groups. On the other hand, compound **14** has a HOMO with electron clouds over the phenyl and tolyl groups in addition to the two nitrogen and oxygen of imidazolone, whereas its LUMO is charged throughout the molecule except for the tolyl group and alkyl group. Furthermore, the HOMO of compound **17** displays electron clouds that are distributed across the entirety of the molecule with the exception of the alkyl group, while the LUMO distributes charges throughout the molecule except for the alkyl and methylbenzyl groups.[37]

Furthermore, using the B3LYP/6-31G(d,p) basis sets, Mulliken atomic charges and electronic populations were calculated. Electron attraction from atoms with a greater electronegative causes the delocalization of negative charges in atoms with lower electronegative values. Carbon atoms contain both positive and negative charges, as seen in Fig. 6. The heteroatoms (N and O) have a high electron density and a negative charge.

**2.2.2. Comparative study between X-ray single crystal and theoretical studies.** Table 2 shows the crystallographic and structure refinement data for compound **11**, and Fig. 7 shows the ORTEP of the molecule with the thermal ellipsoids drawn with 50% probability (CCDC: 2310940). Table S1 (ESI†) provides a summary of the bond length, bond angles, and torsion angles. The crystallization of compound **11** occurs in the monoclinic space group $P2_1/n$. The crystal structure of compound **41** has parameters $a = 6.7814\ (4)$ Å, $b = 10.6880\ (7)$ Å, and $c = 29.8384\ (18)$ Å. Fig. 8 illustrates the three-dimensional packing structure of compound **11**, viewed in the *a*-, *b*-, and *c*-directions.

Fig. 7A shows the ORTEP diagram of compound **11** in the solid state, which displays the atomic numbering. The bond lengths and angles can be found in Table S1 (ESI†). It is noteworthy that the computed data is produced from the isolated gaseous phase, while the experimental data is produced from the solid state. Fig. 9 and 10 illustrates a remarkable agreement between theoretical calculations and X-ray analysis of structural molecular geometry.[38]

**2.2.3. Hirshfeld surface analysis.** Fig. 11 shows the Hirshfeld surfaces for compound **11**, and Fig. 12 shows both the decomposed $d_{norm}$ maps and the 2D-fingerprint plot outlining all potential interactions in compound **11**. The surface color codes in $d_{norm}$ can be used to analyze the molecular interactions, with white regions indicating contacts around the van der Waals radii with the red and blue regions representing shorter and longer inter contacts, respectively. The red and blue triangles in the shape index are a clear indication of the π···π interactions. Additionally, the presence of the flat green region encircled by a blue edge provided additional proof for the π···π interactions.[39] Curvedness maps are used to highlight common packing configurations, such as planar stacking arrangements.[40] For compound **11**, the surface characteristics were mapped across $d_{norm}$ (0.0130–1.371 Å), shape index (1.0–1.0 Å), and curvedness (4.0–0.4 Å). The distance between the surface and the closest atom is $d_e$ in the outer zone of the surface and $d_i$ in the inner zone. The most interactions were H···H interactions, which had a narrow point spike at $d_i + d_e \sim 1.1$ Å and a contact percentage of 64%. Additionally, the percentage contacts of the C···H, H···C, N···H, C···C, O···H, and H···O interactions were 15.5, 12.4, 2.3, 1.6, 1 and 0.8% with narrow point spikes observed at $d_i + d_e \sim 2.8$, 2.8, 3.0, 3.4, 3.0 and 3.0 Å, respectively.

## 2.3. Biological activity

**2.3.1. Insecticidal activity.** The insecticidal activities of compounds **5**, **7**, **9**, **10**, **11**, **14** and **17** were measured against healthy late third instar larvae *P. interpunctella* and *Nilaparvata lugens* according to the standard test[41,42] with a slight modification. The test analogs were dissolved in DMF and serially


© 2024 The Author(s). Published by the Royal Society of Chemistry

Open Access Article. Published on 02 April 2024. Downloaded on 2/13/2026 1:16:18 AM.
This article is licensed under a Creative Commons Attribution-NonCommercial 3.0 Unported Licence.

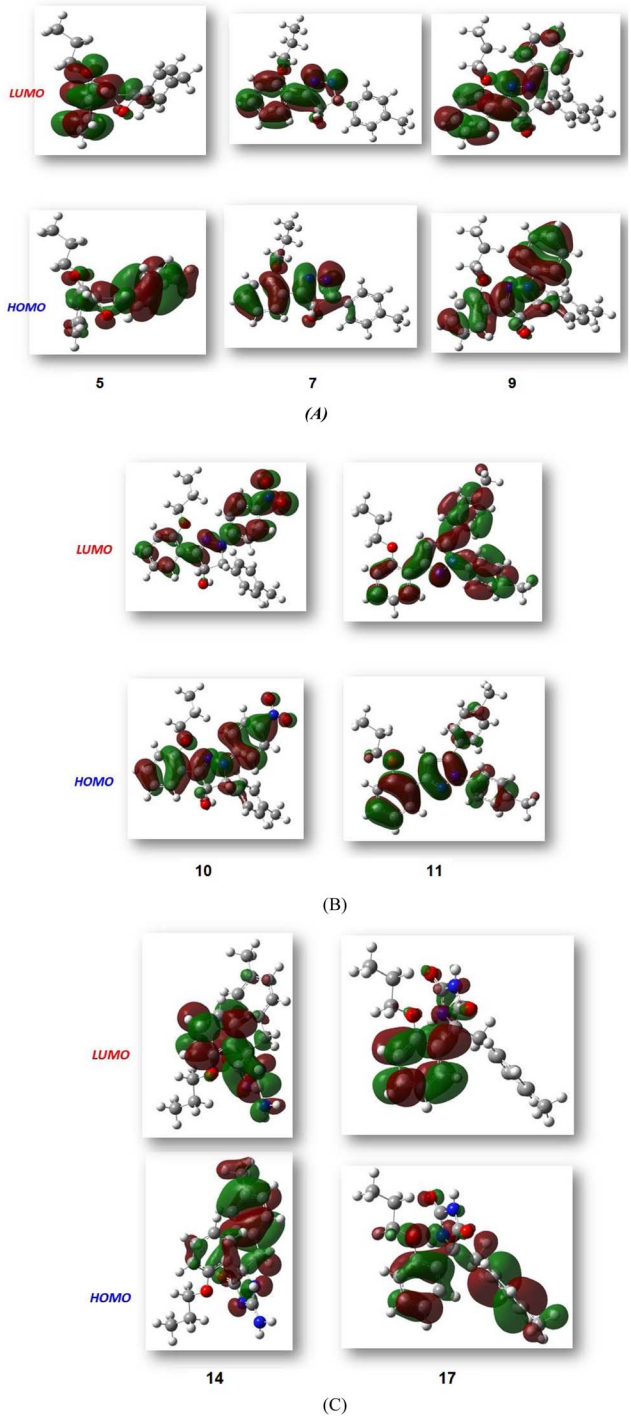


Fig. 5 (A–C) FMO profiles of the synthesized heterocyclic compounds **5**, **7**, **9**, **10**, **11**, **14** and **17**.

diluted with water containing Triton X-80 (0.1 mg $L^{-1}$) to obtain the required concentrations. The insects were reared at 25(±1) ° C and groups were transferred to glass Petri dishes. All experiments were carried out in three replicates for statistic requirements. Assessments of mortality were calculated 48 h by the number and size of the live insects relative to those in the negative control. Evaluations were based on a percentage scale of (0 = no activity and 100 = complete eradication). The mortality rates were subjected to probity analysis.[43] Thiamethoxam was used as a positive control while water-containing Triton X-80 (0.1 mg $L^{-1}$) was used as a negative control. The results shown in Fig. 13 and Table S2 (ESI†) indicated that most of the compounds showed good insecticidal activity against the two pests. For example, compounds **5**, **9**, **10**, and **17** were the most effective against both *P. interpunctella* and *Nilaparvata lugens* at 400 g $mL^{-1}$ with nearly 100% activity. The remaining compounds showed moderate insecticidal activity. For example, compounds **5**, **9**, **10**, and **17** had 100%, 100%, 96.6%, and 100% activities at 400 μg $mL^{-1}$, respectively, against *P. interpunctella*, whereas thiamethoxam had 100%. Furthermore, compounds **5**, **9**, **10**, and **17** exhibited 82%, 86.6%, 83.3%, and 85.3% activities against *Nilaparvata lugens* at 400 μg $mL^{-1}$, respectively, whereas thiamethoxam exhibited 86.6% activity. The authors believed that the trypsin enzymes of *P. interpunctella* larvae were inhibited by compounds **5**, **9**, **10**, **17** and thiamethoxam control, which also demonstrated the capacity to bind to chitin.

The structure–activity relationship (SAR) strategy tries to identify relationships between the biological activity of the examined compounds and their chemical structure. It appears that the presence of an oxirane ring in chalcone **5** contributes significantly to its activity. This is primarily because the ring is easily cleaved, resulting in the formation of an OH group. The OH group plays a pivotal role by readily interacting with OH groups within the biological systems of insects. The confirmation of the interaction is supported by an increase in the activity of compound 1-phenyl-3-(2-propoxyphenyl)-5-(*p*-tolyl)-4,5-dihydro-1*H*-pyrazol-4-ol (**9**). The presence of only the OH group and the blocking of NH through the phenyl ring in compound **9** leads to a greater delocalization of electrons and increased their action compared to compound **7**. Furthermore, compound 1-(4-nitrophenyl)-3-(2-propoxyphenyl)-5-(*p*-tolyl)-4,5-dihydro-1*H*-pyrazol-4-ol (**10**) displays potent activity due to the presence of a withdrawing group, which effectively abstracts electrons, enhancing the attachment of the OH group to the insect cell line through electrostatic hydrogen bond interactions. On the other hand, compounds **11** and **14** exhibit reduced activity compared to the standard drug due to the absence of OH groups in the system, which decrease their action. Finally, compound 5-(4-methylbenzyl)-5-(2-propoxyphenyl)imidazolidine-2,4-dione (**17**) is noteworthy due to the presence of an imidazoline and dione system. This unique feature allows for the easy conversion to an OH group, consequently increasing its electrostatic hydrogen attraction potential. As a result, this compound exhibits heightened activity against *P. interpunctella* and *Nilaparvata*, as displayed in Fig. 13.

The $LC_{50}$ values of compounds **5**, **9**, **10**, and **17** were subject to further evaluation, and the results are presented in Tables 3 and 4. It is noteworthy that the $LC_{50}$ values of compounds **9** and **17** for *P. interpunctella* are notably lower than that of thiamethoxam, suggesting their superior activity compared to the standard reference. In contrast, the $LC_{50}$ value of compound **5** for *Nilaparvata lugens* is also lower than that of thiamethoxam, indicating its enhanced efficacy against *Nilaparvata lugens* when compared to the standard reference.

© 2024 The Author(s). Published by the Royal Society of Chemistry

Open Access Article. Published on 02 April 2024. Downloaded on 2/13/2026 1:16:18 AM.
This article is licensed under a Creative Commons Attribution-NonCommercial 3.0 Unported Licence.

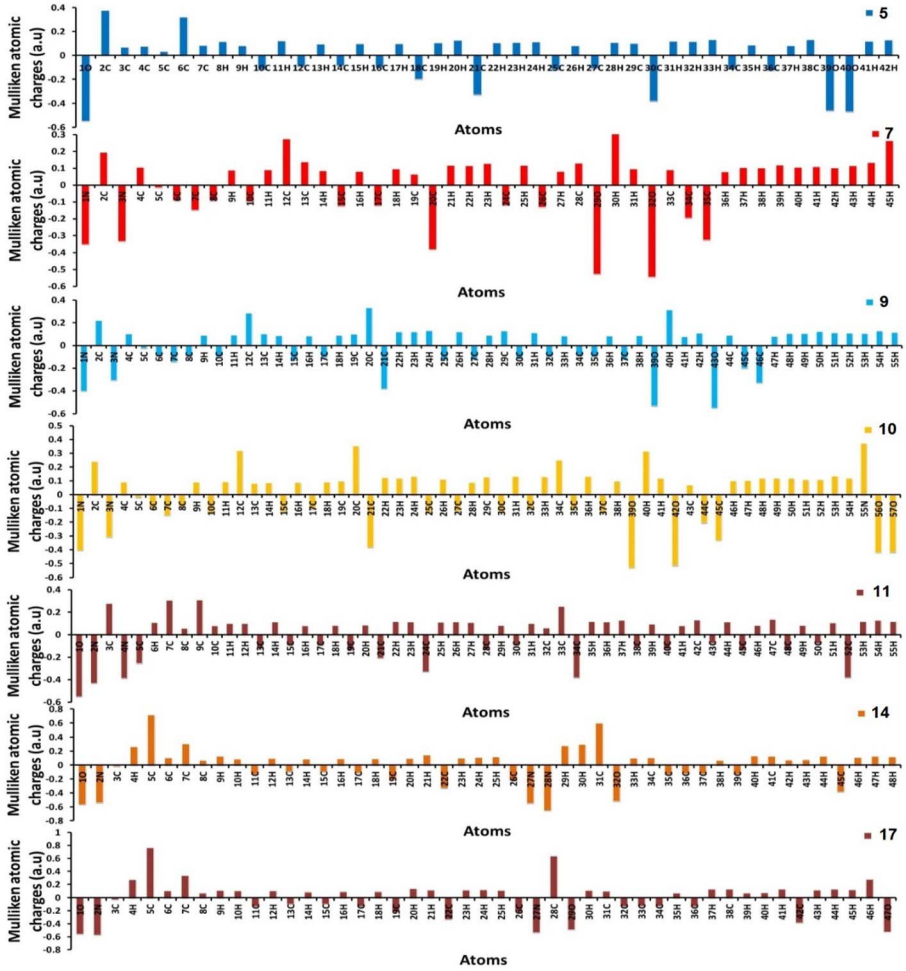


Fig. 6 Distribution of calculated Mulliken charges for compounds **5**, **7**, **9**, **10**, **11**, **14**, and **17**.

**2.3.2. Docking simulation.** The docking studies of **5**, **7**, **9**, **10**, **11**, **14** and **17** using the MOE software[44] to classify the biological effect of the most active compounds of nitrogen heterocyclic compounds compatible with the experimental results. The docking of **5**, **7**, **9**, **10**, **11**, **14** and **17** with different protein receptors, for instance, the crystal structure of *Plodia interpunctella* beta-GRP/GNBP3 N-terminal domain (PDBID: 3aqy)[45] and high resolution structure of *Thermus thermophilus* enoyl-acyl carrier protein reductase NAD and triclosan-form (PDBID: 3wyw).[46] The docking results are elucidated in Fig. 14 and Table 5, which showed the interaction of these nitrogen heterocycles' with PDBID: 3aqy(A). Compound **5** showed high binding energy −8.44 kcal mol$^{-1}$ and its length 2.75 Å with Arg 81, Lys 54, Arg 48, Thr 59 and showed the attachment of C=O of chalcone.[47] Additionally, compounds **9** and **10** showed binding tendency with −8.53, −8.87 kcal mol$^{-1}$ and the presence of OH attract the amino acids with shortage distance between them 1.4, 2.53, and 3.4 Å, while compound **7** displayed a binding energy of −7.32 kcal mol$^{-1}$ and attached with NH pyrazole and OH groups, resulting in bond lengths of 2.65, 2.72, and 3.03 Å (Arg 61, Arg 48, Arg 63). Moreover, compounds **11** and **14** exhibited moderate binding energies of −7.56 and −8.01 kcal mol$^{-1}$ and high length range of 3.04–2.43 Å. On the other hand, compound **17** showed enhanced activity inside the pocket of protein with a high binding energy of −9.03 kcal-mol$^{-1}$ (Thr 59, Arg 61, Ile 50) and had a bond length of 1.59 Å, as displayed in Fig. 14(A) and Table 5. These findings align with the biological results and underscore the significance of compound **17** that possess two C=O and NH groups, which increase the intermolecular interaction due to the presence of more hydrogen bond interactions. Furthermore, Fig. 14(B) and Table 5 also showed the action of compounds **5**, **9**, **10** and **17** with a high binding affinity of −8.34, −8.94, −8.62 and −9.23 kcal mol$^{-1}$, respectively, and attachment with them at the active site position with PDBID: 3wyw(B), which increase its biological evaluation.

# 3. Experimental section

## 3.1. General procedure

The Gallenkamp melting point instrument was used to measure the melting points. Thin-layer chromatography (TLC) was conducted on Polygram SIL G/UV254 TLC plates, and the results were visualized with ultraviolet light at 254 nm and 350 nm. A


© 2024 The Author(s). Published by the Royal Society of Chemistry

Open Access Article. Published on 02 April 2024. Downloaded on 2/13/2026 1:16:18 AM.
This article is licensed under a Creative Commons Attribution-NonCommercial 3.0 Unported Licence.

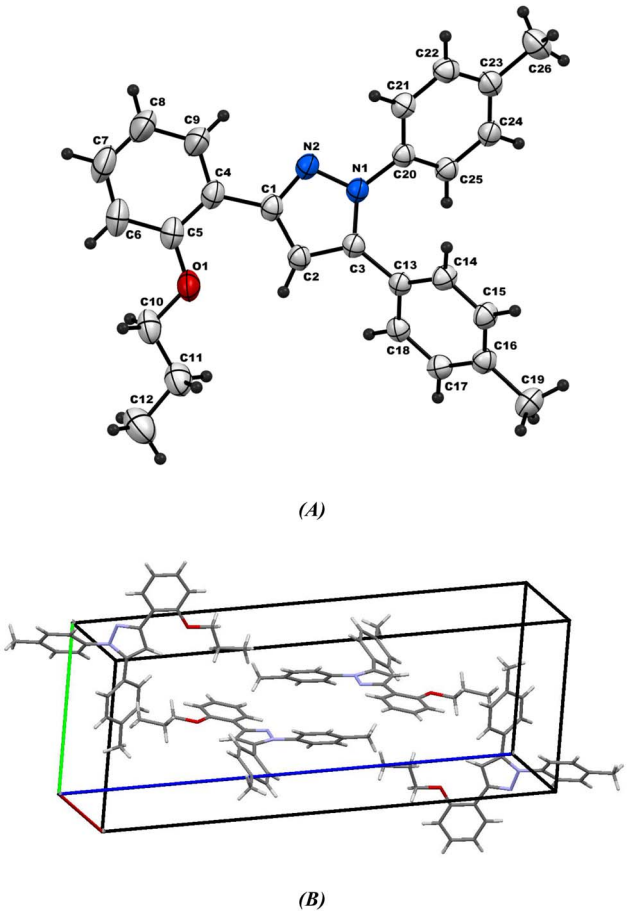


Fig. 7 (A) Ortep-3 crystal structure diagram of compound **11** and (B) unit cell.

Bruker DPX 400 superconducting NMR spectrometer was used to record the $^{1}$H and $^{13}$C nuclear magnetic resonance (NMR) spectra, and the IR spectra were measured with a Jasco Fourier transform/IR-6300 FT-IR spectrometer. The Elementar Vario MICRO Cube was used for elemental analysis. Electron impact (EI) was used to determine mass analyses on a Thermo double-focusing sector (DFS) mass spectrometer. A Varian Cary 5 spectrometer and a Shimadzu UV2600 spectrophotometer were used in UV-vis studies. Utilizing X-ray microdiffraction and single-crystal X-ray diffractometers, Rigaku D/MAX Rapid II and Bruker X8 Prospector were used to determine the X-ray crystal structure.

### 3.2. Materials and reagents

In this study, all solvents and materials were obtained from Aldrich. The synthesis of chalcone **1** was reported in the literature.[48,49]

**3.2.1. Synthesis of (*E*)-1-(2-propoxyphenyl)-3-(*p*-tolyl)prop-2-en-1-one (4).** A mixture of chalcone **1** (1 g, 4.2 mmol), potassium carbonate (1.16 g, 8.4 mmol, 2 equiv.) and 1-bromopropane (4.6 mmol, 1.1 equiv.) in 20 mL of DMF was stirred and refluxed for 16 h. After the reaction was completed, the reaction mixture was poured into water and then the solution was extracted with EtOAc (2 × 20 mL) and washed with water. The organic layer was dried over $MgSO_4$ and evaporated under reduce pressure to give brown oil. Yield (1.1 g, 94%). FT-IR ($\nu_{max}$, cm$^{-1}$): 3026 (C–H Ar), 1657 (C=O), 1601 (C=C), 1568 (ArC–C–). $^{1}$H NMR (DMSO-$d_6$, $\delta$ ppm): 0.89 (t, 3H, $J$ = 7.2 Hz, $H_3$C), 1.68 (m, 2H, $H_2$C), 2.32 (s, 3H, $H_3$C), 4.03 (t, 2H, $J$ = 6.0 Hz, $H_2$C), 7.02 (t, 1H, $J$ = 7.2 Hz, ArH), 7.15 (d, 1H, $J$ = 8.4 Hz, ArH), 7.23 (d, 2H, $J$ = 8.0 Hz, ArH),7.40–7.53 (m, 5H, ArH, C*H*),7.59 (d, 1H, $J$ = 8.0 Hz, C*H*), $^{13}$C NMR (DMSO-$d_6$): $\delta$ 10.44 ($CH_3$), 20.73 ($CH_3$), 21.10 ($CH_2$), 69.59 ($CH_2$), 112.97 (*C*H), 120.63 (*C*H), 126.11 (*C*H), 128.84 (*C*H), 129.02 (*C*H), 129.64 (*C*), 131.86 (*C*), 133.05 (*C*H), 140.42 (*C*), 142.01 (*C*H), 157.25 (*C*), 191.62 (*C*O). MS ($m/z$): 280 ($M^+$, 60%), anal. calcd. for $C_{19}H_{20}O_2$ (280.15): C, 81.40; H, 7.19. Found: C, 81.41%; H, 7.12%.

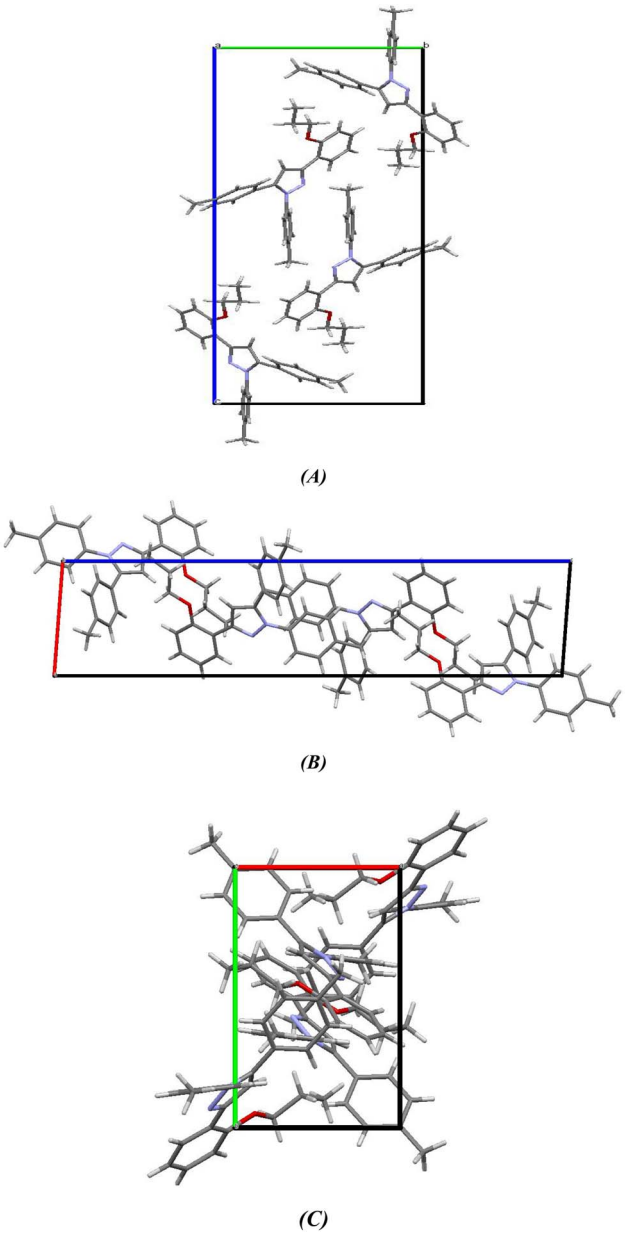


Fig. 8 Three-dimensional packing model of chromenopyridine **11** along the (A) *a*-, (B) *b*- and (C) *c*-direction.

Open Access Article. Published on 02 April 2024. Downloaded on 2/13/2026 1:16:18 AM.
This article is licensed under a Creative Commons Attribution-NonCommercial 3.0 Unported Licence.

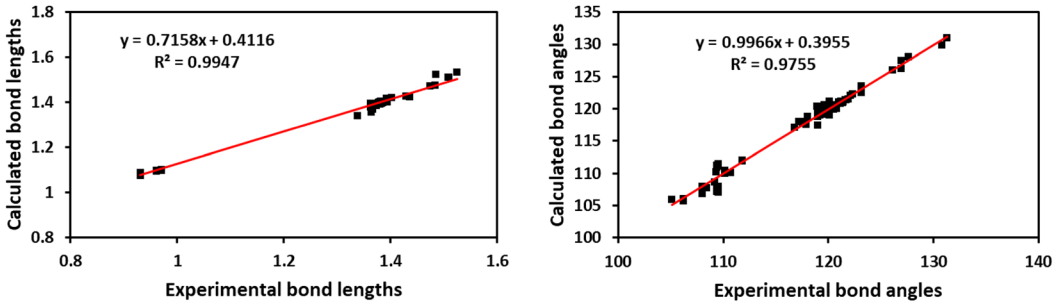


Fig. 9 Correlation graphic between the experimental and calculated bond lengths and bond angles of compound **11**.

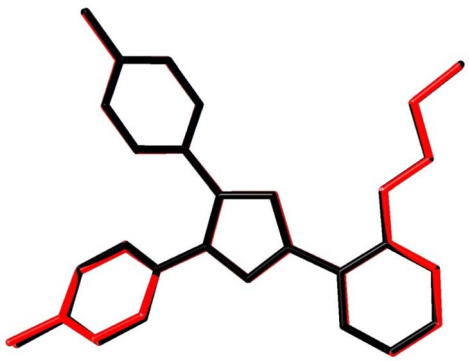

Fig. 10 Atom-by-atom superimposition of compound **11** calculated using DFT/6-31G(d,p) (red) over the X-ray structure (black). Hydrogen atoms are omitted for clarity.

**3.2.2. Synthesis of (2-propoxyphenyl)(3-(*p*-tolyl)oxiran-2-yl) methanone (5).** A solution of chalcone **4** (3 g, 10.7 mmol) in acetone (10 mL) and methanol (10 mL) was mixed with 10% sodium hydroxide (10 mL), followed by the dropwise addition of hydrogen peroxide (30%, 10 mL) at 0 °C. The solution was stirred at room temperature for 1 h, then allowed to stand overnight at room temperature; a precipitate of the α-keto epoxide was formed. The residue was filtered, washed with water and recrystallized from EtOH. Yield (2.9 g, 94.5%), Mp 97–99 °C. FT-IR ($\nu_{max}$, $cm^{-1}$): 3073 (C–H Ar), 1670 (C=O) 1597 (ArC–C–). $^1$H NMR (DMSO-$d_6$, $\delta$ ppm): 0.583 (t, 3H, $J$ = 7.2 Hz, $H_3$C), 1.13 (m, 2H, $H_2$C), 2.32 (s, 3H, $H_3$C), 3.82 (m, 2H, $H_2$C), 4.00 (d, 1H, $J$ = 1.6 Hz, C*H* oxirane), 4.49 (d, 1H, $J$ = 1.6 Hz, C*H* oxirane), 7.05 (t, 1H, $J$ = 7.6 Hz, ArH), 7.14 (d, 1H, $J$ = 8.4 Hz, ArH), 7.20 (d, 2H, $J$ = 8.0 Hz, ArH), 7.27 (d, 2H, $J$ = 8.0 Hz, ArH), 7.56 (t, 1H, $J$ = 8.0 Hz, ArH), 7.67 (d, 1H, $J$ = 7.6 Hz, ArH), $^{13}$C NMR (DMSO-$d_6$): $\delta$ 10.29 ($CH_3$), 20.79 ($CH_3$), 21.28 ($CH_2$), 58.88 (*C*H), 63.19 ($CH_2$), 69.63 (*C*H), 113.15 (*C*H), 120.58 (*C*, *C*H), 125.66 (*C*H), 126.11 (*C*H), 128.89 (*C*H), 129.84 (*C*), 133.21 (*C*H), 135.00 (*C*), 138.12 (*C*), 158.72 (*C*O). MS (*m*/*z*): 296 ($M^+$, 56%), anal. calcd for $C_{19}H_{20}O_3$ (296.14): C, 77.00; H, 6.80. Found: C, 77.01%; H, 6.79%.

**3.2.3. General synthesis of 7–11.** In absolute ethanol (20 mL), oxirane 5 (1 g, 3.37 mmol), and the appropriate hydrazine, namely, hydrazine hydrate or phenyl hydrazine salts (3.37 mmol), were refluxed for 3 hours. The solvent was evaporated under reduced pressure, and the residue was purified by crystallization from ethanol/ether mixture (2 : 1).

*3.2.3.1. Synthesis of 3-(2-propoxyphenyl)-5-(p-tolyl)-4,5-dihydro-1H-pyrazol-4-ol (7).* White solid. Yield (0.4 g, 40%); Mp 130–131 °C. FT-IR ($\nu_{max}$, $cm^{-1}$): 3263 (NH), 3157 (OH), 2963 (aliphatic CH), 1597 (C=N). $^1$H NMR (DMSO-$d_6$, $\delta$ ppm): 0.79 (t, 3H, $J$ = 7.6 Hz, $H_3$C), 1.57 (m, 2H, $H_2$C), 2.29 (s, 3H, $H_3$C), 3.87 (m, 2H, $H_2$C), 4.42 (dd, 1H, $J$ = 2.8 Hz, O*H*, $D_2O$ exchangeable), 5.16 (t, 1H, $J$ = 6.4 Hz, C*H*), 5.38 (d, 1H, $J$ = 6.8 Hz, C*H*), 6.91 (t, 1H, $J$ = 7.2 Hz, ArH), 6.97 (d, 1H, $J$ = 4.4 Hz, ArH), 7.13 (d, 2H, $J$ = 8.0 Hz, ArH), 7.19 (d, 2H, $J$ = 8.0 Hz, ArH), 7.28 (m, 1H, ArH), 7.45 (d, 1H, $J$ = 2.4 Hz, N*H*, $D_2O$ exchangeable), 7.52 (d, 1H, $J$ = 7.6 Hz, ArH), $^{13}$C NMR (DMSO-$d_6$): $\delta$ 10.91 ($CH_3$), 21.09 ($CH_3$), 22.38 ($CH_2$), 70.04 (*C*H), 75.61 ($CH_2$), 79.21 (4), 113.26 (*C*H), 118.20 (*C*H), 120.76 (*C*H), 125.39 (*C*H), 125.89 (*C*H), 129.79 (*C*H), 130.89 (*C*), 133.33 (*C*), 158.45 (*C*), 161.33 (*C*). MS (*m*/*z*): 310 ($M^+$,

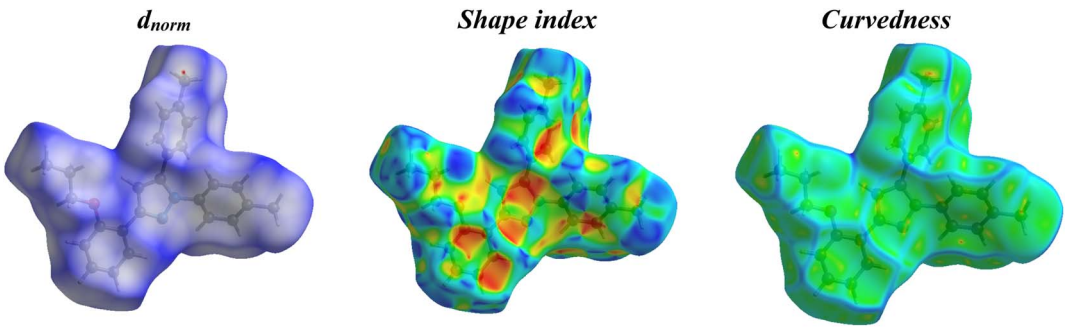


Fig. 11 Hirshfeld surfaces ($d_{norm}$, shape index, and curvedness) of compound **11**.


© 2024 The Author(s). Published by the Royal Society of Chemistry

Open Access Article. Published on 02 April 2024. Downloaded on 2/13/2026 1:16:18 AM.
This article is licensed under a Creative Commons Attribution-NonCommercial 3.0 Unported Licence.

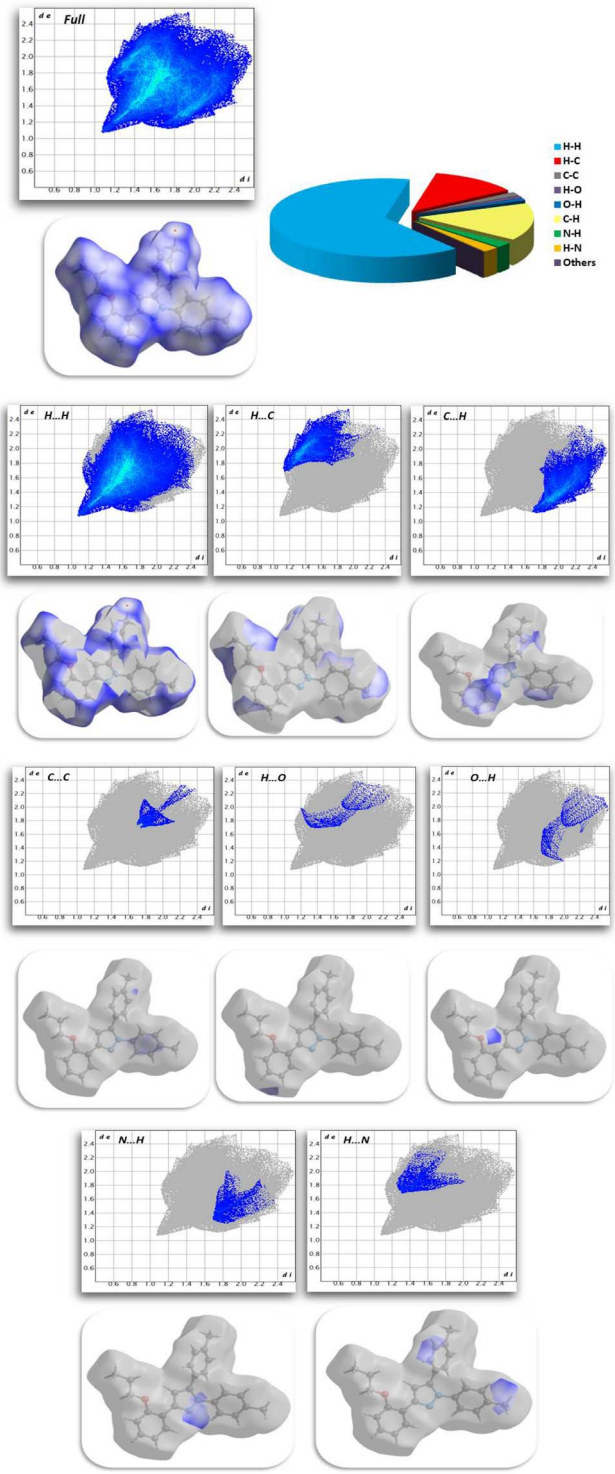


Fig. 12 Selected fingerprint plots and $d_{norm}$ surfaces for important interactions in compound **11**.

30%), anal. calcd for $C_{19}H_{22}N_2O_2$ (310.17): C, 73.52; H, 7.14; N, 9.03. Found: C, 73.50%; H, 7.13%, N, 9.00%.

*3.2.3.2. Synthesis of 1-phenyl-3-(2-propoxyphenyl)-5-(p-tolyl)-4,5-dihydro-1H-pyrazol-4-ol (**9**).* Off white solid. Yield (0.6 g, 46%); m.p 93–95 °C. FT-IR ($\nu_{max}$, $cm^{-1}$): 3538 (OH), 2965

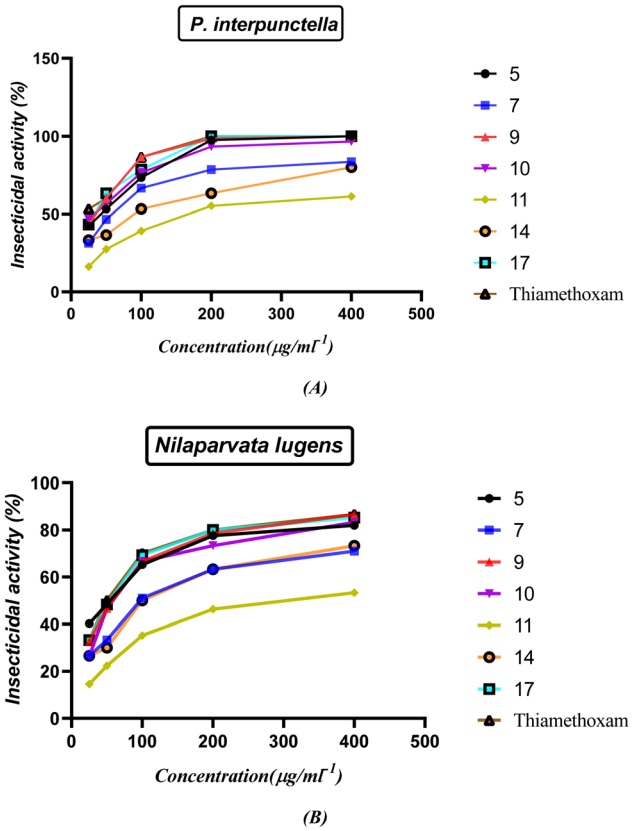


Fig. 13 (A and B) Insecticidal activity of the synthesized nitrogen heterocycles at different concentrations.

(aliphatic CH), 1595 (C=N). $^1$H NMR (DMSO-$d_6$, $\delta$ ppm): 0.74 (t, 3H, $J$ = 7.6 Hz, $H_3$C), 1.55 (m, 2H, $H_2$C), 2.25 (s, 3H, $H_3$C), 3.87 (m, 2H, $H_2$C), 5.05 (d, 1H, $J$ = 2.8 Hz, C*H*), 5.19 (dd, 1H, $J$ = 6.4 Hz, C*H*), 5.97 (d, 1H, $J$ = 7.2 Hz, O*H*, $D_2O$ exchangeable), 6.70 (t, 1H, $J$ = 8.4 Hz, ArH), 6.98 (m, 4H, ArH), 7.01 (m, 6H, ArH), 7.31 (t, 1H, $J$ = 6.8 Hz, ArH), 7.73 (dd, 1H, $J$ = 7.6 Hz, ArH), $^{13}$C NMR (DMSO-$d_6$): $\delta$ 10.37 ($CH_3$), 20.63 ($CH_3$), 21.97 ($CH_2$), 69.47 (*C*H), 71.34 ($CH_2$), 83.52 (*C*H), 112.54 (*C*H), 118.55 (*C*H), 120.35 (*C*), 120.81 (*C*H), 125.76 (*C*H), 128.90 (*C*H), 129.41 (*C*H), 129.58 (*C*H), 129.88 (*C*H), 136.15 (*C*), 136.53 (*C*), 143.71 (*C*), 148.51 (*C*), 156.62 (*C*). MS (*m*/*z*): 386 ($M^+$, 50%), anal. calcd for $C_{25}H_{26}N_2O_2$ (386.20): C, 77.69; H, 6.78; N, 7.25. Found: C, 77.63%; H, 6.76%, N, 7.20%.

*3.2.3.3. Synthesis of 1-(4-nitrophenyl)-3-(2-propoxyphenyl)-5-(p-tolyl)-4,5-dihydro-1H-pyrazol-4-ol (**10**).* Red crystal. Yield (0.4 g, 56%); m.p 162–165 °C. FT-IR ($\nu_{max}$, $cm^{-1}$): 3395 (OH), 2951 (aliphatic CH), 1594 (C=N). $^1$H NMR (DMSO-$d_6$, $\delta$ ppm): 1.04 (t, 3H, $H_3$C), 1.67 (m, 2H, $H_2$C), 2.25 (s, 3H, $H_3$C), 3.95 (m, 2H, $H_2$C), 4.03 (dd, 1H, $J$ = 11.6 Hz, C*H*), 4.35 (broad, 1H, O*H*, $D_2O$ exchangeable), 5.64 (dd, 1H, $J$ = 4.4 Hz, C*H*), 7.01–7.15 (m, 8H, ArH), 7.39 (t, 1H, $J$ = 7.6 Hz, ArH), 7.91 (dd, 1H, $J$ = 2 Hz, ArH), 8.04 (d, 2H, $J$ = 9.6 Hz, ArH), $^{13}$C NMR (DMSO-$d_6$): $\delta$ 10.59 ($CH_3$), 20.64 ($CH_3$), 21.99 ($CH_2$), 46.47 (*C*H), 61.78 ($CH_2$), 69.67 (*C*H), 111.80 (*C*H), 112.96 (*C*H), 120.16 (*C*), 120.57 (*C*H), 125.48 (*C*H), 125.76 (*C*H), 128.75 (*C*H), 129.70 (*C*H), 131.45 (*C*H), 136.99 (*C*), 137.69 (*C*), 138.20 (*C*), 148.26 (*C*), 152.07 (*C*), 157.17 (*C*). MS (*m*/

Open Access Article. Published on 02 April 2024. Downloaded on 2/13/2026 1:16:18 AM. This article is licensed under a Creative Commons Attribution-NonCommercial 3.0 Unported Licence.

Table 3 $LC_{50}$ values of some nitrogen heterocyclic against *P. interpunctella*

| Compound number | $Y = a + bx$ | $LC_{50}$ (mg $L^{-1}$) | 95% limits | Toxic ratio |
|---|---|---|---|---|
| **5** | $Y = 0.1479X + 50.42$ | 1.867 | 0.00 | 0.9745 |
| **9** | $Y = 0.1317X + 57.29$ | 1.428 | 2.647 | 0.9787 |
| **10** | $Y = 0.1253X + 54.52$ | 1.784 | 3.008 | 0.9823 |
| **17** | $Y = 0.1333X + 56.37$ | 1.556 | 2.756 | 0.9811 |
| Thiamethoxam | $Y = 0.1191X + 61.33$ | 1.686 | 0.00 | 0.9504 |

*z*): 431 ($M^+$, 10%), anal. calcd for $C_{25}H_{25}N_3O_4$ (431.18): C, 69.59; H, 5.84; N, 9.74. Found: C, 69.56%; H, 5.81%, N, 9.72%.

*3.2.3.4. Synthesis of 3-(2-propoxyphenyl)-1,5-di-p-tolyl-1H-pyrazole (**11**).* White crystal in DMSO and brown oil at room temperature. Yield (0.4 g, 62%). FT-IR ($\nu_{max}$, $cm^{-1}$): 2963 (aliphatic CH), 1600 (C=N). $^1$H NMR (DMSO-$d_6$, $\delta$ ppm): 1.03 (t, 3H, $H_3$C), 1.83 (m, 2H, $H_2$C), 2.26 (s, 3H, $H_3$C), 2.28 (s, 3H, $H_3$C), 4.05 (m, 2H, $H_2$C), 6.94–7.03 (m, 2H, ArH), 7.04 (s, 1H, C*H*), 7.10–7.22 (m, 6H, ArH), 7.88 (d, 2H, $J$ = 8.4 Hz, ArH), $^{13}$C NMR (DMSO-$d_6$): $\delta$ 10.53 ($CH_3$), 21.06 ($2CH_3$), 22.22 ($CH_2$), 69.91 ($CH_2$), 108.09 (*C*H), 113.08 (*C*H), 120.87 (*C*), 121.67 (*C*H), 124.15 (*C*H), 125.47 (*C*H), 126.89 (*C*H), 127.89 (*C*H), 128.30 (*C*H), 128.69 (*C*), 129.59 (*C*H), 129.93 (*C*), 137.47 (*C*), 137.96 (*C*), 143.33 (*C*), 148.29 (*C*), 156.47 (*C*). MS (*m*/*z*): 382 ($M^+$, 70%), anal. calcd for $C_{26}H_{26}N_2O$ (382.20): C, 81.64; H, 6.85; N, 7.32. Found: C, 81.60%; H, 6.82%, N, 7.30%.

**3.2.4. Synthesis of 2-amino-5-(4-methylbenzyl)-5-(2-propoxyphenyl)-1,5-dihydro-4*H*-imidazol-4-one (14).** Guanidine hydrochloride (0.13 g, 1.35 mmol) and KOH (0.15 g, 2.7 mmol) were added to a solution of epoxychalcone **5** (0.4 g, 1.35 mmol) in ethanol (10 mL). The reaction mixture was refluxed for 3 h. The reaction mixture was filtered, and the solvent was removed using a rotatory evaporator afforded compound 42 (0.24 g, 52%) as a dark yellow solid and recrystallized from EtOH; m.p. 127 °C (decomposed). FT-IR ($\nu_{max}$, $cm^{-1}$): 3265 (NH), 3055 (aromatic CH), 2966 (aliphatic CH), 1656(C=O), 1598 (C=N). $^1$H NMR (DMSO-$d_6$, $\delta$ ppm): 1.08 (t, 3H, $H_3$C), 1.94 (m, 2H, $H_2$C), 2.25 (s, 3H, $H_3$C), 2.92 (d, 1H, $J$ = 12.8 Hz, C$H_2$-A), 3.32 (d, 1H, $J$ = 12.8 Hz, C$H_2$–B), 3.99 (m, 2H, $H_2$C), 6.89 (t, 1H, $J$ = 7.6 Hz, ArH), 7.02 (s, 4H, ArH), 7.06 (d, 1H, $J$ = 8.0 Hz, ArH), 7.26 (t, 1H, $J$ = 8.0 Hz, ArH), 7.37 (s, 1H, NH, $D_2O$ exchangeable), 7.63 (dd, 1H, $J$ = 7.6 Hz, ArH), $^{13}$C NMR (DMSO-$d_6$): $\delta$ 10.58 ($CH_3$), 20.58 ($CH_3$), 22.03 ($CH_2$), 41.71 ($CH_2$), 69.14 ($CH_2$), 69.42 (*C*), 112.25 (*C*), 119.88 (*C*H), 126.03 (*C*H), 126.49 (*C*H), 128.11 (*C*H), 128.71 (*C*H), 130.01 (*C*H), 132.99 (*C*), 135.09 (*C*), 156.43 (*C*), 170.24 (*C*), 187.36 (*C*O). MS (*m*/*z*): 337 ($M^+$, 20%), anal. calcd for $C_{20}H_{23}N_3O_2$ (337.18): C, 71.19; H, 6.87; N, 12.45. Found: C, 71.15%; H, 6.84%, N, 12.42%.

**3.2.5. Synthesis of 5-(4-methylbenzyl)-5-(2-propoxyphenyl) imidazolidine-2,4-dione (17).** Urea (0.101 g, 1.68 mmol) and KOH (0.095 g, 1.68 mmol) were added to a solution of epoxychalcone **5** (0.5 g, 1.68 mmol) in ethanol (10 mL). The reaction mixture was refluxed for 3 h. The reaction mixture was filtered, and the solvent was removed using a rotatory evaporator, then rescrystallized with EtOH which afforded compound **17** (0.1 g, 17%) as an off-white solid; m.p. 235–237 °C. FT-IR ($\nu_{max}$, $cm^{-1}$): 3356, 3195 (NH), 3068 (aromatic CH), 2957 (aliphatic CH), 1763 (C2=O), 1717 (C4=O). $^1$H NMR (DMSO-$d_6$, $\delta$ ppm): 0.89 (t, 3H, $H_3$C), 1.64 (m, 2H, $H_2$C), 2.28 (s, 3H, $H_3$C), 3.18 (d, 1H, $J$ = 13.2 Hz, C$H_2$-A), 3.40 (d, 1H, $J$ = 13.2 Hz, C$H_2$-B), 3.86 (m, 2H, $H_2$C), 6.96 (t, 1H, $J$ = 8.4 Hz, ArH), 7.04 (d, $J$ = 8 Hz, 1H, ArH), 7.09 (s, 4H, ArH), 7.33 (t, 1H, $J$ = 7.6 Hz, ArH), 7.56 (d, 1H, $J$ = 7.6 Hz, ArH), 7.85 (s, 1H, NH, $D_2O$ exchangeable), 10.09 (s, 1H, NH, $D_2O$ exchangeable), $^{13}$C NMR (DMSO-$d_6$): $\delta$ 10.45 ($CH_3$), 20.61 ($CH_3$), 21.58 (*C*H), 40.00 ($CH_2$), 65.42 ($CH_2$), 69.72 (*C*), 112.26 (*C*), 119.81 (*C*H), 127.06 (*C*H), 127.31 (*C*H), 128.30 (*C*H), 129.54 (*C*H), 130.52 (*C*H), 131.46 (*C*), 135.63 (*C*), 156.64 (*C*O), 156.88 (*C*), 176.25 (*C*O). MS (*m*/*z*): 338 ($M^+$, 8%), anal. calcd for $C_{20}H_{22}N_2O_3$ (338.16): C, 70.99; H, 6.55; N, 8.28. Found: C, 70.98%; H, 6.52%, N, 8.24%.

### 3.3. Hirshfeld surface analysis

The topology analyses were performed using Crystal Explorer 17.5 program.[50]

### 3.4. Computational studies

Molecular geometry was directly taken from the experimental outcomes of X-ray diffraction without any constraints. Density functional theory including Becke's three-parameter hybrid functional using the LYP correlation functional (B3LYP) with the 6-31G(d,p) basis set *via* the Berny method[34,35] were proceeded with the Gaussian 09W program.[51] The superimposition was performed using Olex2.[52] Furthermore, the Mullikan atomic charges of compounds **5**, **7**, **9**, **10**, **11**, **14** and **17** were calculated as well.

Table 4 $LC_{50}$ values of some nitrogen heterocycles against *Nilaparvata lugens*

| Compound number | $Y = a + bx$ | $LC_{50}$ (mg $L^{-1}$) | 95% limits | Toxic ratio |
|---|---|---|---|---|
| **5** | $Y = 0.1575X + 31.66$ | 1.567 | 1.324 to 1.811 | 0.9937 |
| **9** | $Y = 0.1762X + 28.57$ | 1.720 | 1.613 to 1.830 | 0.9987 |
| **10** | $Y = 0.1714X + 26.86$ | 1.727 | 1.482 to 1.991 | 0.9924 |
| **17** | $Y = 0.1720X + 30.29$ | 1.670 | 1.500 to 1.845 | 0.9964 |
| Thiamethoxam | $Y = 0.1727X + 30.86$ | 1.655 | 1.505 to 1.809 | 0.9972 |


© 2024 The Author(s). Published by the Royal Society of Chemistry

Open Access Article. Published on 02 April 2024. Downloaded on 2/13/2026 1:16:18 AM.
This article is licensed under a Creative Commons Attribution-NonCommercial 3.0 Unported Licence.

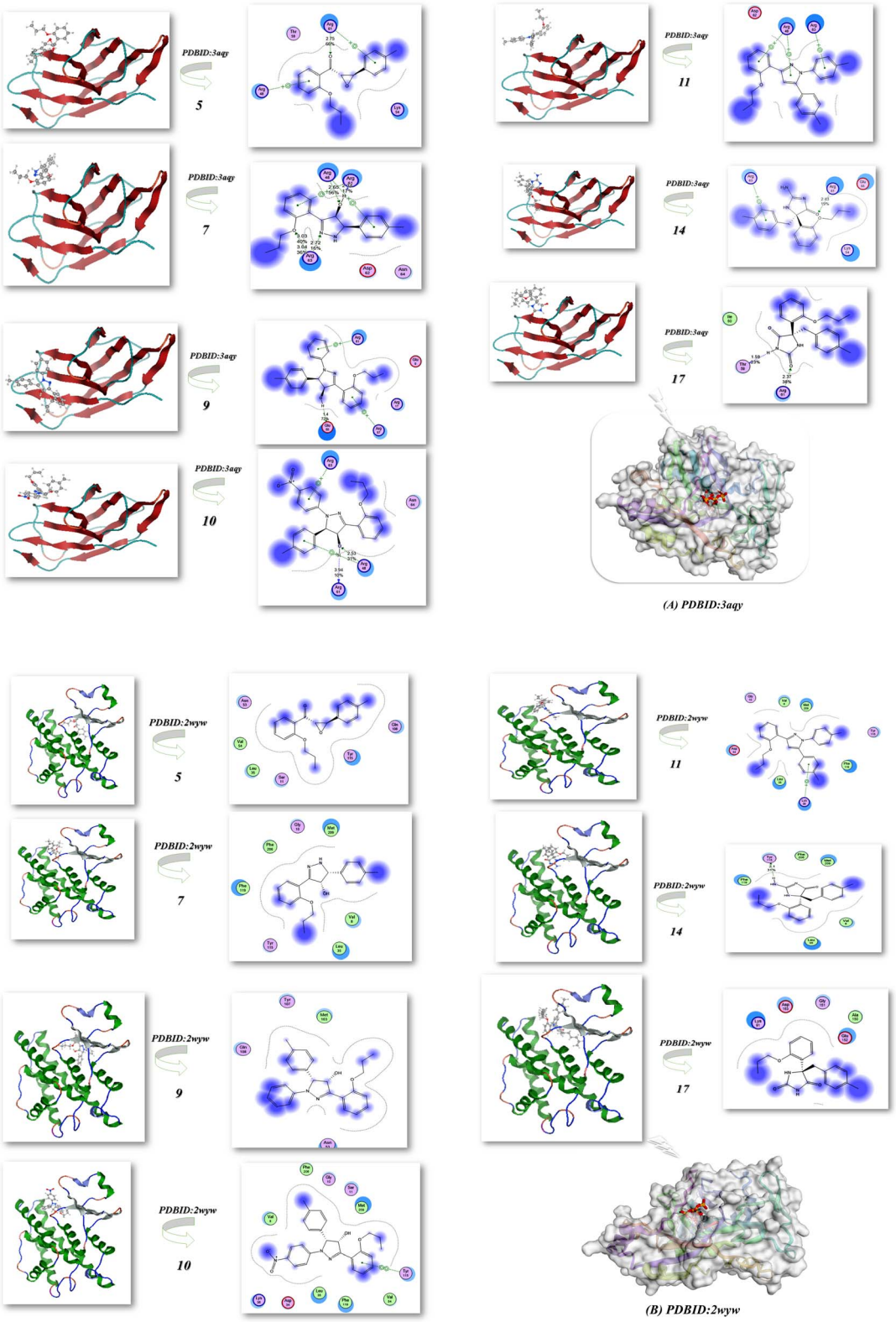


Fig. 14 (A and B) Docking analysis of the nitrogen nucleophile with PDBID: 3aqy and PDBID: 3wyw.

### 3.5. Insecticidal activity

**3.5.1. Evaluation of insecticidal action of heterocycles against larvae of *P. interpunctella* and *Nilaparvata lugens*.** Laboratory-reared insect colonies of *P. interpunctella* and *Nilaparvata lugens* free from insecticides and pathogens obtained from Insect 14 S. A. RIZK ET AL. greenhouse of Pest control

Open Access Article. Published on 02 April 2024. Downloaded on 2/13/2026 1:16:18 AM. This article is licensed under a Creative Commons Attribution-NonCommercial 3.0 Unported Licence.

Table 5 Docking simulation heterocycle derivatives with different PDBIDs: 3aqy, 3wyw

| | *Escherichia coli* (PDBID: 3aqy) | | | | *Streptococcus pneumoniae* (PDBID: 3wyw) | | |
|---|---|---|---|---|---|---|---|
| | Energy affinity (kcal mol$^{-1}$) | Distance (Å) | Amino acids | | Energy affinity (kcal mol$^{-1}$) | Distance (Å) | Amino acids |
| **5** | −8.44 | 2.75 Å | Arg 81, Lys 54, Arg 48, Thr 59 | **5** | −8.34 | −2.01 Å | Tyr 115, Gln 108, Ser 11, Leu 35, Val 54, Asn 53 |
| **7** | −7.32 | 2.65, 2.72, 3.03 Å | Arg 61, Arg 48, Arg 63 | **7** | −7.11 | 2.54 Å | Leu 35, Val 8, Tyr 115, Gly 10, Met 209, Phe 206, Phe 119 |
| **9** | −8.53 | 1.4 Å | Glu 55, Arg 57, Arg 17, Glu 9, Arg 61 | **9** | −8.94 | 2.23 Å | Tyr 107, Met 103, Gln 108, Asn 53 |
| **10** | −8.87 | 2.53, 3.4 Å | Arg 63, Asn 64, Arg 48, Arg 61 | **10** | −8.62 | 2.11 Å | Tyr 115, Val 54, Phe 11, Leu 35, Ser 11, Met 209, Phe 206, sp 34 |
| **11** | −7.56 | 3.04 Å | Arg 48, Arg 63, Asp 62 | **11** | −6.32 | −3.04 Å | Lys 36, Asp 34, Leu 35, Phe 119, Val 54, Tyr 115, Met 209, Ser 11, Gly 10 |
| **14** | −8.01 | 2.43 Å | Arg 63, Arg 61, Glu 55, Lys 54 | **14** | −7.13 | −2.1 Å | Tyr 115, Phe 206, Met 209, Val 8, Leu 35, Phe 119 |
| **17** | −9.032 | 1.59 Å | Thr 59, Arg 61, Ile 50 | **17** | −9.23 | −2.08 Å | Lys 91, Asp 153, Gly 151, Ala 150, Glu 152 |

Analytical lab, Entom-Aysel Company, Cairo, Egypt were maintained starting from egg rafts. The collected populations of *P. interpunctella* were reared in plates on an artificial diet comprised of soybean flour, yeast powder, casein, dry maize leaf powder, cholesterol, sugar, agar, ascorbic acid, sorbic acid, methyl *p*-hydroxybenzoate, vitamin solution, and distilled water, while collected populations of *N. lugens* were reared on rice (*Oryza sativa* L.) seedlings (7–10 days after germination) in the laboratory with controlled conditions, such as temperature 37 ± 1 °C and 70–80% relative humidity with a 16–8 h (L/D) photoperiod. The third nymph instars of the second laboratory generation were used for bioassays.[53,54]

**3.5.2. Docking analysis.** Utilizing the MOE software, novel compounds were molecularly docked,[44] and the Discovery Studio Client (version 4.2) was used to find it.[55] The energy of the obtained conformations decreased using the Confirmation Examination module of Auto Dock Vina after systematic conformational research was undertaken out to an RMS gradient of 0.01. The crystal structure of *Plodia interpunctella* beta-GRP/GNBP3 N-terminal domain (PDBID: 3aqy)[45] was determined and the structural characterization of the catalytic site of a *Nilaparvata lugens* delta-class glutathione transferase (PDBID: 3wyw)[56] was done. Ten distributed docking simulations were performed using default parameters, and the confirmations were generated based on the organization of the overall data, the *E* conformation, and the appropriate use of the pertinent amino acids in each protein's binding pocket.

### 3.6. Crystal information

CCDC 2310940 is the ESI Publication Number† for the crystallographic data deposited at the Cambridge Crystallographic Data Centre.

## 4. Conclusion

In conclusion, our research involves the effective synthesis of several pyrazole and imidazole derivatives. A variety of analytical and spectroscopic techniques were used to confirm their identity and structural characterization. Moreover, we utilized DFT calculations and X-ray analysis to optimize and validate the synthesized compounds' structures, affirming their accuracy. In terms of biological activity, compounds **5**, **9**, **10**, and **17** displayed remarkable insecticidal potential, surpassing the performance of the standard reference thiamethoxam. Docking simulations with specific proteins further supported their efficacy, highlighting their strong binding interactions with amino acids.

## Conflicts of interest

There are no conflicts to declare.

## Acknowledgements

Dr Mohammad H. BinSabt gratefully acknowledges the resources of the research sector projects unit (RSPU) general facilities of the Faculty of Science (GFS) (GS03/08) of Kuwait University for X-ray analysis.

## References

1 B. Kaur and P. Singh, *Bioorg. Chem.*, 2022, **125**, 105862.
2 Y. Hu, C. Li, B. A. Kulkarni, G. Strobel, E. Lobkovsky, R. M. Torczynski and J. A. Porco, *Org. Lett.*, 2001, **3**, 1649–1652.
3 G. Thirunarayanan and G. Vanangamudi, *Spectrochim. Acta, Part A*, 2011, **81**, 390–396.
4 A. Singh, A. Raza, S. Amin, C. Damodaran and A. K. Sharma, *Molecules*, 2022, **27**, 886.
5 A. M. Fahim, E. H. I. Ismael and H. E. M. Tolan, *Polycyclic Aromat. Compd.*, 2023, 1–42.
6 B. S. Lane and K. Burgess, *Chem. Rev.*, 2003, **103**, 2457–2474.
7 D.-G. Crivoi, A. M. Segarra and F. Medina, *J. Catal.*, 2016, **334**, 120–128.


© 2024 The Author(s). Published by the Royal Society of Chemistry

Open Access Article. Published on 02 April 2024. Downloaded on 2/13/2026 1:16:18 AM. This article is licensed under a Creative Commons Attribution-NonCommercial 3.0 Unported Licence.

8 H. Yi, G. Zou, Q. Li, Q. Chen, J. Tang and M.-y. He, *Tetrahedron Lett.*, 2005, **46**, 5665–5668.
9 M. Zhang, T. Chen, S. Fang, W. Wu, X. Wang, H. Wu, Y. Xiong, J. Song, C. Li, Z. He and C.-S. Lee, *Org. Biomol. Chem.*, 2021, **19**, 2481–2486.
10 J. Liu, F. Li, Z. Hao, Y. Wang, X. Hua, Y. Li and Z. Li, *Bioorg. Med. Chem.*, 2020, **28**, 115829.
11 F. Tanaka, Y. Magariyama and A. Miyanoshita, *Food Chem.*, 2020, **303**, 125381.
12 M. M. Khan, Q. Huang, T. A. Wagan, H. Hua, W. Cai and J. Zhao, *J. Asia-Pac. Entomol.*, 2020, **23**, 269–276.
13 M. Calvo-Agudo, J. González-Cabrera, D. Sadutto, Y. Picó, A. Urbaneja, M. Dicke and A. Tena, *Environ. Pollut.*, 2020, **267**, 115581.
14 P. Maienfisch, M. Angst, F. Brandl, W. Fischer, D. Hofer, H. Kayser, W. Kobel, A. Rindlisbacher, R. Senn, A. Steinemann and H. Widmer, *Pest Manage. Sci.*, 2001, **57**, 906–913.
15 S. A. Rizk, A. Y. Alzahrani and A. M. Abdo, *Polycyclic Aromat. Compd.*, 2023, 1–18, DOI: **10.1080/10406638.2023.2227316**.
16 R. Yang, T. Xu, J. Fan, Q. Zhang, M. Ding, M. Huang, L. Deng, Y. Lu and Y. Guo, *Ind. Crops Prod.*, 2018, **117**, 50–57.
17 J. Wu, B.-A. Song, D.-Y. Hu, M. Yue and S. Yang, *Pest Manage. Sci.*, 2012, **68**, 801–810.
18 S. P. Chandrasekharan, A. Dhami, S. Kumar and K. Mohanan, *Org. Biomol. Chem.*, 2022, **20**, 8787–8817.
19 K. Karrouchi, S. Radi, Y. Ramli, J. Taoufik, Y. N. Mabkhot, F. A. Al-aizari and M. h. Ansar, *Molecules*, 2018, **23**, 134.
20 A. M. Vinggaard, U. Hass, M. Dalgaard, H. R. Andersen, E. Bonefeld-Jørgensen, S. Christiansen, P. Laier and M. E. Poulsen, *Int. J. Androl.*, 2006, **29**, 186–192.
21 Y. Gao, D.-C. Huang, C. Liu, Z.-L. Song, J.-R. Liu, S.-K. Guo, J.-Y. Tan, R.-L. Qiu, B. Jin, H. Zhang, N. Mulholland, X. Han, Q. Xia, A. S. Ali, D. Guo, Y. Deng, Y.-C. Gu and M.-Z. Zhang, *Bioorg. Med. Chem.*, 2021, **35**, 116073.
22 B. D. Tonietto, A. O. M. Laurentino, M. T. Costa-Valle, L. V. Cestonaro, B. P. Antunes, C. Sates, N. G. dos Santos, E. Dallegrave, S. C. Garcia, M. B. Leal and M. D. Arbo, *Environ. Toxicol. Pharmacol.*, 2022, **94**, 103924.
23 M. A. Shalaby, A. M. Fahim and S. A. Rizk, *Sci. Rep.*, 2023, **13**, 4999.
24 E. Weitz and A. Scheffer, *Ber. Dtsch. Chem. Ges.*, 1921, **54**, 2327–2344.
25 Y. Apeloig, M. Karni and Z. Rappoport, *J. Am. Chem. Soc.*, 1983, **105**, 2784–2793.
26 L. Knorr and A. Blank, *Ber. Dtsch. Chem. Ges.*, 1884, **17**, 2049–2052.
27 E. C. Cipagauta Esquivel, V. C. Rufino, M. H. Trindade Nogueira, A. C. Carbonaro Souza, J. R. Pliego Júnior and M. S. Valle, *J. Mol. Struct.*, 2020, **1204**, 127536.
28 D. Nair, P. Pavashe, S. Katiyar and I. N. N. Namboothiri, *Tetrahedron Lett.*, 2016, **57**, 3146–3149.
29 S. Laufer, G. Wagner and D. Kotschenreuther, *Angew. Chem., Int. Ed.*, 2002, **41**, 2290–2293.
30 C. Zhang, S. Sarshar, E. J. Moran, S. Krane, J. C. Rodarte, K. D. Benbatoul, R. Dixon and A. M. M. Mjalli, *Bioorg. Med. Chem. Lett.*, 2000, **10**, 2603–2605.
31 K. Faghihi, K. Zamani, A. Mirsamie and M. Reza Sangi, *Eur. Polym. J.*, 2003, **39**, 247–254.
32 B. A. Bhat, K. L. Dhar, S. C. Puri and M. Spiteller, *Synlett*, 2006, **2006**, 2723–2726.
33 L. Varga, T. Nagy, I. Kövesdi, J. Benet-Buchholz, G. Dormán, L. Ürge and F. Darvas, *Tetrahedron*, 2003, **59**, 655–662.
34 C. Peng, P. Y. Ayala, H. B. Schlegel and M. J. Frisch, *J. Comput. Chem.*, 1996, **17**, 49–56.
35 H. B. Schlegel, *J. Comput. Chem.*, 1982, **3**, 214–218.
36 A. Mohamed, A. M. Fahim and M. A. Ibrahim, *J. Mol. Model.*, 2020, **26**, 354.
37 N. A. Kheder, A. M. Fahim, N. S. Mahmoud and K. M. Dawood, *J. Mol. Struct.*, 2024, **1295**, 136772.
38 M. N. Ahmed, H. Andleeb, A. M. Fahim, M. Madni, S. W. Khan, B. Kaboudin, M. A. A. Ibrahim, P. A. Sidhom and D. M. Gil, *J. Mol. Struct.*, 2024, **1296**, 136908.
39 H. A. Ghabbour, A. M. Fahim, M. A. Abu El-Enin, S. T. Al-Rashood and H. A. Abdel-Aziz, *Mol. Cryst. Liq. Cryst.*, 2022, **742**, 40–55.
40 S. Madhankumar, P. Muthuraja and M. Dhandapani, *J. Mol. Struct.*, 2019, **1181**, 118–130.
41 J. Ma, S. Tong, P. Wang, W. Liao, H. Liu and L. Zhang, *J. Econ. Entomol.*, 2010, **103**, 492–496.
42 Z.-P. Che, J.-M. Yang, X.-J. Shan, Y.-E. Tian, S.-M. Liu, X.-M. Lin, J. Jiang, M. Hu and G.-Q. Chen, *J. Asian Nat. Prod. Res.*, 2020, **22**, 678–688.
43 X. Zheng and J. Polli, *Eur. J. Pharm. Sci.*, 2010, **41**, 43–52.
44 S. Vilar, G. Cozza and S. Moro, *Curr. Top. Med. Chem.*, 2008, **8**, 1555–1572.
45 M. Kanagawa, T. Satoh, A. Ikeda, Y. Adachi, N. Ohno and Y. Yamaguchi, *J. Biol. Chem.*, 2011, **286**, 29158–29165.
46 J. M. Otero, A.-J. Noel, P. Guardado-Calvo, A. L. Llamas-Saiz, W. Wende, B. Schierling, A. Pingoud and M. J. van Raaij, *Acta Crystallogr., Sect. F*, 2012, **68**, 1139–1148.
47 A. M. Fahim, S. Dacrory and G. H. Elsayed, *Sci. Rep.*, 2023, **13**, 14563.
48 B. M. Ivković, K. Nikolic, B. B. Ilić, Ž. S. Žižak, R. B. Novaković, O. A. Čudina and S. M. Vladimirov, *Eur. J. Med. Chem.*, 2013, **63**, 239–255.
49 M. A. Shalaby, H. M. Al-Matar, A. M. Fahim and S. A. Rizk, *J. Phys. Chem. Solids*, 2022, **170**, 110933.
50 P. R. Spackman, M. J. Turner, J. J. McKinnon, S. K. Wolff, D. J. Grimwood, D. Jayatilaka and M. A. Spackman, *J. Appl. Crystallogr.*, 2021, **54**, 1006–1011.
51 M. J. Frisch, G. W. Trucks, H. B. Schlegel, G. E. Scuseria, M. A. Robb, J. R. Cheeseman, G. Scalmani, V. Barone, B. Mennucci, G. A. Petersson, H. Nakatsuji, M. Caricato, X. Li, H. P. Hratchian, A. F. Izmaylov, J. Bloino, G. Zheng, J. L. Sonnenberg, M. Hada, M. Ehara, K. Toyota, R. Fukuda, J. Hasegawa, M. Ishida, T. Nakajima, Y. Honda, O. Kitao, H. Nakai, T. Vreven, J. A. Montgomery, J. E. Peralta, F. Ogliaro, M. Bearpark, J. J. Heyd, E. Brothers, K. N. Kudin, V. N. Staroverov, R. Kobayashi, J. Normand, K. Raghavachari, A. Rendell, J. C. Burant, S. S. Iyengar, J. Tomasi, M. Cossi, N. Rega, N. J. Millam, M. Klene, J. E. Knox, J. B. Cross, V. Bakken, C. Adamo, J. Jaramillo, R. E. R. Gomperts, O. Stratmann, A. Yazyev,

Open Access Article. Published on 02 April 2024. Downloaded on 2/13/2026 1:16:18 AM.
This article is licensed under a Creative Commons Attribution-NonCommercial 3.0 Unported Licence.

J. Austin, R. Cammi, C. Pomelli, J. W. Ochterski, R. L. Martin, K. Morokuma, V. G. Zakrzewski, G. A. Voth, P. Salvador, J. J. Dannenberg, S. Dapprich, A. D. Daniels, Ö. Farkas, J. B. Foresman, J. V. Ortiz, J. Cioslowski and D. J. Fox, Gaussian, Inc., Wallingford, CT, USA, 2009.

52 O. V. Dolomanov, L. J. Bourhis, R. J. Gildea, J. A. Howard and H. Puschmann, *J. Appl. Crystallogr.*, 2009, **42**, 339–341.

53 R. Xu, R. Xia, M. Luo, X. Xu, J. Cheng, X. Shao and Z. Li, *J. Agric. Food Chem.*, 2014, **62**, 381–390.

54 X. Yu, Y. Liu, Y. Li and Q. Wang, *J. Agric. Food Chem.*, 2015, **63**, 9690–9695.

55 S. Vilar, G. Cozza and S. Moro, *Curr. Top. Med. Chem.*, 2008, **8**, 1555–1572.

56 K. Yamamoto, A. Higashiura, M. D. T. Hossain, N. Yamada, T. Shiotsuki and A. Nakagawa, *Arch. Biochem. Biophys.*, 2015, **566**, 36–42.


© 2024 The Author(s). Published by the Royal Society of Chemistry